Antioxidants & Redox Signaling

Antioxidants & Redox Signaling: http://mc.manuscriptcentral.com/liebert/ARS

Activation of endogenous H2S biosynthesis or supplementation with exogenous H2S enhances adipose tissue adipogenesis and preserves adipocyte physiology in humans

Journal:	*Antioxidants and Redox Signaling*
Manuscript ID	ARS-2020-8206.R2
Manuscript Type:	Original Research Communication
Date Submitted by the Author:	22-Jan-2021
Complete List of Authors:	Comas, Ferran ; IDIBGI, Nutrition, eumetabolism and health Latorre, Jèssica; IDIBGI Ortega, Francisco; IDIBGI Arnoriaga Rodríguez, Maria; IDIBGI Kern, Matthias; University of Leipzig Faculty of Medicine Lluch, Aina; IDIBGI Ricart, Wifredo; Hospital of Girona, Endocrinology Blüher, Matthias; University of Leipzig Faculty of Medicine Gotor, Cecilia; Instituto de Bioquímica Vegetal y Fotosíntesis Romero, Luis ; Instituto de Bioquímica Vegetal y Fotosíntesis Fernández-Real, José; Institut d'Investigació Biomédica de Girona (IdIBGi), Department of Diabetes, Endocrinology and Nutrition Moreno-Navarrete, José María; IDIBGI,
Keyword:	Hydrogen Sulfide, Post-translational protein modifications
Manuscript Keywords (Search Terms):	adipogenesis, obesity, adipose tissue, hydrogen sulfide, Protein persulfidation

Comas

Activation of endogenous H_2S biosynthesis or supplementation with exogenous H_2S enhances adipose tissue adipogenesis and preserves adipocyte physiology in humans

Ferran Comas[1], Jèssica Latorre[1], Francisco Ortega[1], María Arnoriaga Rodríguez[1], Matthias Kern[2], Aina Lluch[1], Wifredo Ricart[1], Matthias Blüher[2], Cecilia Gotor[3], Luis C. Romero[3], José Manuel Fernández-Real[1,4*], José María Moreno-Navarrete[1,4*]

[1]Department of Diabetes, Endocrinology and Nutrition, Institut d'Investigació Biomèdica de Girona (IdIBGi), CIBEROBN (CB06/03/010) and Instituto de Salud Carlos III (ISCIII), Girona, Spain.

[2]Department of Medicine, University of Leipzig, Leipzig, Germany.

[3]Instituto de Bioquímica Vegetal y Fotosíntesis, Consejo Superior de Investigaciones Científicas and Universidad de Sevilla, Seville, Spain.

[4]Department of Medicine, Universitat de Girona, Girona, Spain.

Abbreviated Title: H_2S in human adipose tissue adipogenesis

*Corresponding author and person to whom reprint requests should be addressed**:**
J.M. Moreno-Navarrete, Ph.D. e-mail: jmoreno@idibgi.org
J.M. Fernández-Real, M.D. Ph.D. e-mail: jmfreal@idibgi.org
Section of Diabetes, Endocrinology and Nutrition
Hospital of Girona "Dr Josep Trueta"
Carretera de França s/n, 17007, Girona, SPAIN.
Phone: 34-972-94 02 00
Fax: 34-972-94 02 70

Keywords: Adipogenesis, adipose tissue, hydrogen sulfide, obesity, protein persulfidation.

Word count: 4036; number of references: 84; number of greyscale figures: 9; number of color figures: 1 (online 1 and 7).

Comas

Abstract

Aims: To investigate the impact of exogenous hydrogen sulfide (H_2S) and its endogenous biosynthesis on human adipocytes and adipose tissue in the context of obesity and insulin resistance.

Results: Experiments in human adipose tissue explants and in isolated preadipocytes demonstrated that exogenous H_2S or the activation of endogenous H_2S biosynthesis resulted in increased adipogenesis, insulin action, sirtuin deacetylase and PPARγ transcriptional activity, whereas chemical inhibition and gene knockdown of each enzyme generating H_2S (*CTH*, *CBS*, *MPST*) led to altered adipocyte differentiation, cellular senescence and increased inflammation. In agreement with these experimental data, visceral and subcutaneous adipose tissue expression of H_2S-synthesising enzymes was significantly reduced in morbidly obese subjects in association with attenuated adipogenesis and increased markers of adipose tissue inflammation and senescence. Interestingly, weight loss interventions (including bariatric surgery or diet/exercise) improved expression of H_2S biosynthesis-related genes. In human preadipocytes, expression of *CTH*, *CBS* and *MPST* genes and hydrogen sulfide production were dramatically increased during adipocyte differentiation. More importantly, the adipocyte proteome exhibiting persulfidation was characterized, disclosing that different proteins involved in fatty acid and lipid metabolism, the citrate cycle, insulin signalling, several adipokines and PPAR experienced the most dramatic persulfidation (85-98% ~~p<0.0000001~~).

Innovation: No previous studies investigated the impact of H_2S on human adipose tissue. This study suggests that the potentiation of adipose tissue H_2S biosynthesis is a possible therapeutic approach to improve adipose tissue dysfunction in patients with obesity and insulin resistance.

Comas

Conclusion: Altogether these data supported the relevance of H_2S biosynthesis in the modulation of human adipocyte physiology.

Abbreviations

AT, adipose tissue; DDA; data-dependent acquisition; DIA, data-independent acquisition; FDR, False Discovery Rate; HOMA-IR, Homeostasis Model Assessment – Insulin Resistance Index; KD, gene knockdown; LDH, Lactate Dehydrogenase; PLP, pyridoxal 5'-phosphate; PPG, DL-propargylglycine; SAT, subcutaneous adipose tissue; sc, subcutaneous; shRNA, short hairpin RNA; SVF, stromal vascular cells; VAT, visceral adipose tissue.

Comas

Introduction

Adipose tissue dysfunction, characterised by increased inflammation and cellular senescence and reduced adipogenesis, is an important contributor to obesity-associated metabolic disturbances, including insulin resistance (10, 33, 44). Increased oxidative stress and reactive oxygen species (ROS) levels in adipose tissue have been extensively demonstrated in obesity in association to insulin resistance and adipocyte dysfunction (1, 2, 13, 24, 62). The attenuation of adipose tissue oxidative stress might be an important therapeutic approach to prevent adipose tissue dysfunction and improve obesity-associated metabolic disturbances (50).

Hydrogen sulfide (H_2S) is a gaseous mediator that plays important regulatory roles in innate immunity and inflammatory responses impacting on the development of cardiovascular and metabolic diseases (8, 23, 32, 70, 81). In mammalian systems, H_2S is endogenously generated from cysteine by pyridoxal-5'-phosphate (PLP)-dependent enzymes, cystathionine β-synthase (CBS) and cystathionine γ-lyase (CTH or CSE), through the transsulfuration pathway (34), but also in absence of PLP by 3-mercaptopyruvate sulfurtransferase (MPST) that converts 3-mercaptopyruvate into H_2S (39, 68).

H_2S exerts its biological actions attenuating oxidative stress through different molecular mechanisms, including scavenging of ROS (69) and protein persulfidation (63). Protein persulfidation is a post-translational modification in which thiol groups (R–SH) from reactive cysteine residues are converted into perthiols (R–SSH). Persulfidation is known to modulate the structure and biological activity of target proteins, preventing irreversible cysteine overoxidation, and in consequence, preserving protein function (22, 56, 63, 84).

Comas

A recent study reported increased serum sulfide levels in subjects with morbid obesity in positive correlation with fat mass (17), but negatively associated with hyperglycemia (17, 77), showing decreased serum sulfide levels in obese subjects with altered glucose tolerance. In line with this study, previous studies also demonstrated decreased plasma sulfide levels in association to type 2 diabetes (77) or decreased adipose tissue H_2S production capacity in mice models of obesity and diabetes (high fat diet and db/db) (35). In fact, there is emerging evidence in the 3T3-L1 mouse cell line pointing to a possible role of H_2S in adipocyte differentiation through the modulation of PPARγ activity (9, 73, 80). The overexpression of the H_2S generation enzyme CTH and the administration of the H_2S donor NaHS to 3T3-L1 cells in an environment of high glucose restored adiponectin secretion and decreased the secretion of proinflammatory cytokines (59). However, the impact of H_2S on human adipocytes has not been investigated, while its possible role in human adipose tissue physiology and adipogenesis is not yet completely understood.

We here aimed to investigate the possible role of H_2S on human adipogenesis and adipose tissue in the context of obesity and insulin resistance, and report the first observations, to our knowledge, linking H_2S to the physiology of human adipose tissue.

Comas

Results

To examine the impact of H_2S on adipose tissue, *ex vivo* experiments were performed in adipose tissue explants from cohort 1, in which paired SAT and VAT were obtained from 20 morbidly obese participants with different degrees of systemic insulin sensitivity. Anthropometric and clinical parameters are shown in Suppl Table 1. As detailed in methods, the effects of GYY4137 in 5 consecutive participants and induction of endogenous H_2S biosynthesis in all participants (n=20) were tested, ~~being~~ with sulfide levels being analyzed in 8 consecutive participants.

Exogenous H_2S administration increased adipogenesis, sirtuin and PPARγ activity in human adipose tissue explants

The most common class of H_2S donors are the sulfide salts [such as sodium hydrosulfide (NaSH) and sodium sulfide (Na_2S)] and GYY4137. Sulfide salts produced a fast release of H_2S triggering acute supraphysiological effects, and then H_2S levels drop rapidly. In contrast, GYY4137 induces a slower but more prolonged H_2S release, with increased peaking time (10 min vs 10 s for NaSH), but decreased peaking concentration (400-fold lower than for NaSH) (63). In human adipose tissue *ex vivo*, GYY4137 (5 µM, 16h at 37ºC) administration increased *ADIPOQ, FASN, SLC2A4* and *SIRT1* mRNAs in parallel to sulfide levels in tissue culture media (Figure 2A). GYY4137 (200 µM, 1h at 37ºC) also increased sirtuin deacetylase (Figure 2B) and PPARγ transcriptional (Figure 2C) activities in adipose tissue lysates.

Ex vivo stimulation of H_2S biosynthesis enhances the expression of adipogenic genes and *SIRT1* in association with insulin sensitivity

Then, H_2S biosynthesis was examined in human adipose tissue explants (Suppl Table 1), after adding L-cysteine and pyridoxal 5'-phosphate (PLP), known to induce H_2S biosynthesis through CBS and CTH. We observed increased endogenous H_2S

biosynthesis (Figure 2D) in parallel to raised *CTH* and *CBS* mRNAs levels (Table 1, Figure 2E-F), pointing that *CTH* and *CBS* gene expression is associated to H_2S biosynthesis. The induction of endogenous H_2S biosynthesis resulted in increased sulfide levels in tissue culture media and enhanced expression of adipogenic (*ADIPOQ, PPARG, SLC2A4, CIDEA* and *FASN*) and *SIRT1* genes in both subcutaneous (SAT) and visceral (VAT) adipose tissue (Table 1, Figure 2D). Sulfide concentration in the media positively correlated with *ADIPOQ*, *PPARG, SLC2A4* and *SIRT1* gene expression in both SAT and VAT (Figure 2E-F). The increase in SAT, but not VAT, *ADIPOQ, SLC2A4, FASN* and *SIRT1* gene expression after endogenous H_2S biosynthesis induction in AT explants was higher in those morbidly obese participants with decreased Hb1Ac (Figure 3A-D), but increased insulin sensitivity (Figure 3E-H).

Supporting these experimental data, VAT and SAT H_2S-synthesising enzymes (*CTH*, *CBS*, *MPST*) gene expression, which is in association to H_2S biosynthesis, were associated to systemic insulin sensitivity and adipose tissue adipogenesis in two cross-sectional (cohort 2 and 3) and three longitudinal (cohort 4, 5, 6) cohorts, in which bariatric surgery or diet/exercise interventions were performed.

Insulin sensitivity is associated to *CTH* expression in human adipose tissue

In cohort 2, VAT and SAT *CTH*, *CBS* and SAT *MPST* gene expression were significantly decreased in obese subjects (Suppl Table 2, Figure 4A-C) in association with homeostasis model assessment – insulin resistance index (HOMA-IR) and fasting triglycerides (Table 2). HOMA-IR was the main factor contributing to decreased SAT *CTH* (β= -0.29, p=0.04) and SAT *CBS* (β= -0.42, p=0.02) after adjusting for sex, age and body mass index (BMI). In a subgroup of 12 participants, in which CTH protein levels were analysed, a positive correlation between CTH protein and mRNA levels in both SAT and VAT were found (Figure 4D).

Comas

In an independent cohort of morbidly obese participants (cohort 3, Suppl Table 3), insulin sensitivity (euglycemic clamp) was positively correlated with SAT *CTH* (r=0.55, p=0.02, Figure 4E) and *CBS* (r=0.45, p=0.06, Figure 4F), but not *SAT MPST* (r=0.34, p=0.1) after excluding participants with type 2 diabetes. VAT *CTH* gene expression was also negatively correlated with HOMA-IR (Table 3).

Association of *CTH, CBS* and *MPST* with markers of adipose tissue functionality and the effects of weight loss

In cohort 2, in both VAT and SAT, *CTH*, *CBS* and *MPST* gene expression was positively correlated with adipogenic (*FASN, ACACA, PPARG*), insulin signaling pathway-related (*IRS1, SLC2A4*), *SIRT1* and *PPARGC1A* gene expression and negatively associated with expression of *LEP*, *LBP* and *TNF* (only *MPST*) genes (Table 2). In cohort 3, concordant associations were found for *CTH* and *MPST*, but not for *CBS* gene expression (Table 3). *CTH* gene expression correlated with expression of adipogenic (*ADIPOQ, PPARG*), mitochondrial biogenesis (*PPARGC1A*), insulin signaling pathway-related (*IRS1*) genes, and markers of cellular senescence (positively with *SIRT1* and negatively with *BAX, TP53* and *TNF* gene expression (Table 3). *MPST* mRNA also positively correlated with *PPARG, ADIPOQ* and *SLC2A4* genes (Table 3).

In cohort 4, bariatric surgery-induced weight loss resulted in increased *CTH* (29.7%, p=0.0005), *CBS* (9.6%, p=0.05) and *MPST* (15.2%, p=0.01) mRNAs in parallel to improved insulin sensitivity and systemic inflammation (53, 57). Interestingly, the increase in *CTH* mRNA was positively correlated with the increase in *ADIPOQ* (r= 0.71, p= 0.002), *SIRT1* (r= 0.53, p= 0.03) and *PPARGC1A* (r= 0.56, p= 0.02) mRNAs. Similar findings were observed in an independent cohort after bariatric surgery-induced weight loss (cohort 6) and also after diet or exercise-induced weight loss (cohort 5), with increased SAT *CTH* mRNA levels (55% and 29%, respectively, both p<0.01).

Comas

In adipose tissue cell fractions, *CTH* and *MPST* gene expression significantly increased in human adipocytes in comparison with stromal vascular cells (SVF) (Figure 4G-H), whereas no significant differences in *CBS* gene expression between these 2 cell types were detected (Figure 4I).

Expression of H_2S-synthesising enzymes increases with adipocyte differentiation

Next, H_2S biosynthesis was investigated at cellular level, in human preadipocytes and adipocytes. We found that an adipocyte endogenous source of H_2S is prominent in human adipocytes. Sulfide levels were detectable and quantified in the culture media of human adipocytes and consistently increased by a ~30% with adipocyte differentiation (Figure 5A-B). *CTH* and *MPST* gene expression increased progressively during human adipocyte differentiation (Figure 5C-D) in close parallelism with adipogenic genes (*ADIPOQ,* Figure 5E). *CBS* increased slightly only in the last days of differentiation (day 12 and day 14, Figure 5F). These findings were confirmed at the protein level, observing high levels of sulfide-producer enzyme accumulation after differentiation (Figure 5G).

Exogenous H_2S potentiates insulin action and adipogenesis in human adipocytes

GYY4137 had no apparent effects on PPARγ transcriptional activity in preadipocytes (Figure 6A) (72 h) but led to a significantly increased sirtuin deacetylase activity (Figure 6B). In contrast, GYY4137 increased PPARγ transcriptional activity in adipocytes (Figure 6C), without significantly affecting sirtuin deacetylase activity (Figure 6D). GYY4137 treatment resulted in a 3-fold increase ($p<0.001$) in ^{pSer473}Akt/Akt ratio in response to insulin (Figure 6E).

GYY4137 dose-dependently increased the expression of adipogenic genes (*ADIPOQ, FABP4* and *CEBPA*) and *SLC2A4* in the last days of adipocyte differentiation and this effect was reverted by the CTH inhibitor propargylglycine (PPG) (Figure 6F-I).

Comas

Chemical inhibition of H_2S-synthesising enzymes attenuates adipogenesis and impacts inflammation in human adipocytes

Propargylglycine (PPG) is a known specific chemical inhibitor of the CTH enzyme, which led to a significant reduction of intracellular lipid accumulation (Figure 7A), fatty acid synthase protein levels (Figure 7B) and adipogenic gene expression (*ADIPOQ, FABP4, PPARG, FASN, PLIN1*) (Figure 7C-G) during adipogenesis. PPG led to raised markers of cellular senescence (*BAX, TP53*), proinflammatory cytokines (*IL6, TNF*) and ^{pSer536}NFκB (p65)/NFκB (p65) ratio, without changing LDH activity (a direct measure of cellular damage and necrosis) ((Figure 7H-M).

In fully differentiated adipocytes, PPG also attenuated insulin-induced ^{Ser473}Akt phosphorylation (Figure 7N), reduced *ADIPOQ, FASN, DGAT1*, *PPARG*, *IRS1, PPARGC1A* and *SIRT1* (Suppl Figure 1A-G), but did not affect inflammatory or cellular senescence-related gene expression or LDH activity (Suppl Figure 1H-L).

Gene knockdown (KD) of *CTH, CBS* and *MPST* in human preadipocytes impairs adipocyte differentiation

The effects of chemical compounds such as GYY4137 or PPG up- or downregulating H_2S production could be due to off-target mechanisms acting at multiple levels. For this reason, we studied how *CTH, CBS* and *MPST* gene KD affect adipogenesis during human adipocyte differentiation. The silencing of all these genes resulted in significantly decreased expression of adipogenic, lipogenic and insulin pathway-related genes while increasing inflammatory gene expression (Figure 8A-C). *CTH* gene KD resulted in a significantly decreased expression in adipogenic (*ADIPOQ, FABP4, FASN, PPARG, CEBPA*) and insulin pathway (*SLC2A4, IRS1*)-related genes while increasing inflammatory mRNAs (*IL6, TNF*) (Figure 8A). *CBS* gene KD also resulted in decreased *ADIPOQ, FABP4, FASN, CEBPA, SLC2A4* and *IRS1*, and increased *IL6* mRNA levels

Comas

(Figure 8B). *MPST* gene KD led to decreased *ADIPOQ, FABP4, FASN, PPARG, CEBPA* and *SLC2A4*, and increased *IL6* and *TNF* mRNA levels (Figure 8C). Of note, the most antiadipogenic effect was observed in CTH gene KD, since expression of all adipogenic and insulin pathway-related genes was reduced between 45-55% ($p<0.005$).

Persulfidation affects proteins involved in adipogenesis

Between 10-30% of the cellular proteome is susceptible to being modified by persulfidation as it has been reported in mammals and plants, being this a highly prevalent protein post-translational modification (6, 60). For this reason, to gain insight into the mechanism underlying the adipogenic effects of H_2S, whole proteome persulfidation in preadipocytes and adipocytes was analysed and compared. To assess that, a sequential window acquisition of all theoretical spectra-mass spectrometry (SWATH-MS) quantitative approach with the tag-switch method (83) was combined for identification of protein persulfidation in preadipocyte and differentiated human cell cultures. Protein samples from four biological replicates extracted from preadipocyte and differentiated adipocyte cell cultures were isolated and subjected to the chemoselective tag-switch method to label persulfidated proteins. The enriched samples in persulfidated proteins obtained were digested, and the peptide solutions analyzed in two sequential steps: a shotgun data-dependent acquisition (DDA) approach to generate the spectral library, and SWATH acquisition by a data-independent acquisition (DIA) method. In the first step, after integrating the eight datasets, a total of 19,053 peptides [1% false discovery rate (FDR) and 92.8 % confidence] and 2,016 unique proteins (1% FDR) were identified and used as spectral library (Suppl dataset 1, available in PRIDE with identifier PXD018720). In the second step, to quantify protein levels using SWATH acquisition, the same eight biological samples were analyzed twice each (technical replicas) by a DIA method. For quantitation, the fragment spectra were obtained for the sixteen runs and 1,590 proteins

were quantified (Suppl dataset 2, available in PRIDE with identifier PXD018720), of which 954 were differentially more or less abundant in each culture with a fold change of ± 1.5 and p value < 0.05 (Suppl dataset 3, available in PRIDE with identifier PXD018720). From these proteins, 332 proteins were more persulfidated in differentiated adipocytes and in addition, we detected in the spectral library generated by the DDA approach 496 proteins that were only identified in the adipocyte samples and were under the detection limit in preadipocyte cultures (Suppl Table 4). Therefore, a total of 828 proteins were only persulfidated or were more persulfidated in differentiated adipocyte cultures.

In differentiated human adipocytes, persulfidation was significantly increased in proteins involved in fatty acid and lipid metabolism, the citrate cycle, adipokine, PPAR and insulin signalling (Figure 9A-B), Among them, we identified PLIN1, previously described as susceptible of persulfidation (21), which validated the proteomic approach used, and other important proteins and enzymes in adipocyte physiology, such as FASN, SCD, ACACA, THRSP, PLIN4, LIPE, ACSL1, SLC2A4 (GLUT4) and FABP4 (all with p<0.0000001), but not non-adipogenic control proteins, such as ACTB, ENO1 and PARK7 (61) that showed similar level of persulfidation in both cell cultures (Figure 9C). Considering that persulfidation preserved protein integrity and function in conditions of oxidative stress where cysteine residues may be partially oxidized (22, 63, 84), current data suggested that persulfidation in adipocytes might have a crucial role preserving those proteins involved in adipogenesis and adipocyte physiology. These proteins mainly included enzymes, lipid droplet-associated proteins, membrane transporters and receptors that modulate lipogenesis, lipolysis, mitochondrial function and insulin action (Suppl dataset 2 and Figure 9A-B). On the other hand, in preadipocytes the proteins that were persulfidated belonged to pathways involved in immune response, cell migration,

Comas

glycosaminoglycan degradation, complement and coagulation cascades and bacterial invasion of epithelial cells (Suppl Figure 2A-B).

Comas

Discussion

The current study provides sound and novel evidences supporting the importance of H_2S biosynthesis in the physiology of human adipose tissue. Altogether current findings pointed to a crucial role of H_2S and H_2S-synthesizing enzymes in human adipose tissue physiology at different cellular levels. Even though, the specific molecular mechanism to explain the possible effects of H_2S on human adipogenesis has not been fully resolved in this study, some mechanisms might be inferred from current findings. These putative mechanisms were as follows:

i) Preserving adipogenic-related proteins through protein persulfidation. Persulfidation often increases the reactivity of target proteins, modulating their biological activities, whereas other post-translational modifications, such as S-nitrosylation often decreases protein activity (25). In fact, a recent study showed experimentally, for the first time, a higher chemical reactivity in proteins with persulfidated cysteines compared to proteins with cysteines with sulfur in the thiol state (26). Even though, the most reported impact of persulfidation is to activate protein function, some studies demonstrated inhibitory effects in some important proteins (26).

Taking into account that we found increased persulfidation in FASN, SCD, ACACA, THRSP, PLIN4, LIPE, ACSL1, GLUT4 and FABP4, and that an appropriate functionality of these proteins is required for adipogenesis and adipocyte physiology (3, 14, 19, 31, 42, 46, 66, 82), the current results suggest that endogenous H_2S biosynthesis might preserve the function of those proteins involved in adipogenesis. However, further experiments are required to confirm this suggestion.

Supporting the importance of H_2S in the physiology of adipose cells, *CTH*, *CBS* and *MPST* mRNA levels were detected at substantial levels in adipocytes, increasing during human adipocyte differentiation in parallel to *ADIPOQ*. The knockdown of *CTH*, *CBS*

and *MPST* promoted the development of dysfunctional adipocytes during adipocyte differentiation, decreasing markers of adipogenesis and increasing the expression of proinflammatory cytokines in parallel to decreased H_2S biosynthesis. Of note, the most anti-adipogenic effect was observed in *CTH* gene KD. The chemical inhibition of CTH activity resulted in decreased adipogenesis during human adipocyte differentiation and in fully differentiated adipocytes. In fact, anti-adipogenic and inflammatory effects of high PPG dose (250 μM) during human adipocyte differentiation were comparable with the effects of *CTH* gene KD. In contrast, no significant effects of low PPG dose (25 μM) were found. This discrepancy could be explained by the previously reported low potency, low selectivity and the limited cell-membrane permeability of PPG (7). However, considering that inhibiting CBS, CTH and MPST may have effects independent of H_2S, such as perturbations in homocysteine metabolism, the results of PPG or gene knockdown experiments should be interpreted with caution. In addition, it should be considered that knockdown of one of these enzymes might be compensated by H_2S production by the remaining ones. Otherwise, the administration of GYY4137 in the last stage of the process resulted in a dose-dependent increased expression of adipogenic genes. Interestingly, when endogenous H_2S production was inhibited with PPG (250 μM), GYY4137 sustained adipogenic gene expression (Figure 6), preventing the reduction observed in Figure 7. Previous studies demonstrated that adipogenic (73) and anti-cancer (41) effects of GYY4137 were not observed when cells were treated with ZYJ1122, its structural analogue lacking sulfur, indicating that GYY4137 effects were dependent of H_2S moiety. *Ex vivo* experiments also demonstrated that the activation of H_2S-producing enzymes in adipose tissue increased expression of adipogenic genes in correlation to H_2S biosynthesis. Consistent with the suggested impact of H_2S on protein persulfidation in adipose cells (current study), a recent study demonstrated that persulfidation depends on

intracellular H_2S levels, observing in those situations of decreased H_2S biosynthesis, such as aging, a significant decline in protein persulfidation, whereas conditions of enhanced H_2S production (such as dietary restriction) were associated with increased protein persulfidation (84).

ii) *Preventing inflammatory processes in human preadipocytes through the induction of sirtuin deacetylase activity*. Specifically, in human preadipocytes, exogenous H_2S (GYY4137) treatment enhanced sirtuin activity, whereas when endogenous H_2S biosynthesis was inhibited (using PPG or in *CTH, CBS* and *MPST* KD) markers of cellular senescence (*TP53*), apoptosis (*BAX*) and inflammation (*TNF, IL6*) increased. These findings suggest that the previously reported anti-senescence effects of H_2S (20, 51, 65) might contribute to improve the adipogenic function of preadipocytes, and preserve adipose tissue functionality (4). In addition, increased *SIRT1* mRNA levels and sirtuin activity after transsulfuration pathway activation or GYY4137 administration in *ex vivo* experiment (adipose tissue explants) or the consistent association between H_2S-producing enzymes and *SIRT1* gene expression in human adipose tissue reinforced this idea. Furthermore, both SAT and VAT *CTH* gene expression negatively correlated with markers of cellular senescence (*TP53*), inflammation (*TNF*) and apoptosis (*BAX*) in obese subjects, which were all associated to adipose tissue dysfunction and insulin resistance (36, 37, 52, 71). Even though, TP53, inflammatory cytokines (IL6 and TNF) or apoptosis markers has all been previously used to characterize senescence-associated adipose tissue dysfunction (36, 37, 52, 71), a more accurate measurement of cellular senescence (such as β-galactosidase activity) should be considered to confirm current associations in further studies.

Strengthening current findings, increased SIRT1 activity led to enhanced adipose tissue rejuvenation (characterized by increased cellular stemness) and decreased inflammation

Comas

(12, 29, 43, 64, 78) and H_2S administration resulted in enhanced Sirt1 expression and activity (20, 51, 65), preventing vascular aging (20) and cellular senescence in human fibroblasts (65). In line with these findings, in immortalized human adipose-derived mesenchymal stem cells, which unlike human preadipocytes and adipocytes (current study) displayed a much higher expression of CBS than CTH gene (18), *CBS* gene knockdown promotes a cellular senescence phenotype characterized by increased inflammation and oxidative stress, and decreased H_2S production (18). Of note, this cellular senescence phenotype resulted in adipocyte hypertrophy, when these cells differentiated into adipocytes, and attenuated their ability to differentiate into osteogenic linage (18).

iii) *Increasing insulin action through the activation of PPARγ transcriptional activity in differentiated adipocytes*. GYY4137 administration resulted in a significant increase of insulin-induced Akt phosphorylation at serine 473, whereas PPG administration had opposite effects. A fine regulation of insulin action is associated to adipogenesis and adipose tissue physiology (55, 67). *Ex vivo* experiments indicated that the adipogenic effect resulting from transsulfuration pathway activation was increased in association with insulin sensitivity, and negatively correlated with HbA1c levels, supporting the relationship between H_2S and adipose tissue insulin action. In addition, AT *CTH* gene expression was positively correlated to systemic insulin sensitivity in both cross-sectional studies (cohort 1 and cohort 2) and increased after bariatric surgery-induced weight loss similar to insulin sensitivity. H_2S improved insulin action in mice (28, 48, 49, 79). GYY4137 administration improved high fat diet-induced insulin resistance through the activation of PPARγ in adipose tissue, whereas PPG exerted opposite effects (9). Mechanistically, H_2S-induced PPARγ transactivation is mediated by enhanced PPARγ persulfidation in cysteine residues from DNA binding domain (9, 80). Since PPG

Comas

administration also increased ^{pSer536}NFκB (p65)/NFκB ratio and proinflammatory cytokines (*IL6* and *TNF*), another potential mechanism to explain H_2S effects on insulin action was the inhibition of NFκB-induced inflammation (23).

In support of current findings, CBS deficiency is known to be associated with decreased fat mass in both mice and humans (30, 38). CTH is involved in adipogenesis in phylogenetically distant species from drosophila to mice (9, 73, 80) with *cth* knockout mice developing decreased fat mass under cysteine-limited diets (47).

Decreased levels of H_2S-synthesizing enzymes in morbidly obese subjects seems in contradiction with the relevance of these enzymes in adipogenesis and fat mass accretion. However, in conditions of obesity and insulin resistance, adipogenesis is attenuated (40, 54, 74), and size enlargement of pre-existing adipocytes acquires more relevance in fat mass sustaining (45). The findings in human adipose tissue are in agreement with decreased adipose tissue H_2S production reported in db/db and high-fat diet-fed mice (35). Even though, adipose tissue as a possible source of increased serum sulfide levels, recently described in morbidly obese subjects (17), cannot be discarded. Alternative hypothesis should be investigated: i) Expression of H_2S-synthesizing enzymes could be higher in early phases of obesity but decrease in more advanced disease as a consequence of adipose tissue inflammation and insulin resistance. ii) In addition, H_2S production depends not only by the expression/activity of synthesizing enzymes but also on its oxidation. Decreased oxidation may be the result of environmental hypoxia as that present in adipose tissue from subjects with obesity (72). In this context, decreased oxidation could result in persistently higher serum sulfide levels.

Current data might anticipate clinical applications and also suggest that the modulation of adipose tissue H_2S biosynthesis may play a role in glucose metabolism. Dietary raw garlic homogenate (a complex mixture containing several H_2S precursors) administration

restored plasma H_2S levels in diabetic rats and led to increased insulin sensitivity (58). Therapeutically, the potentiation of adipose tissue H_2S-synthesizing enzymes to improve adipose tissue physiology in patients with type 2 diabetes should be investigated in depth in further studies.

Conclusions

This study sustains adipose tissue H_2S-synthesizing enzymes as important actors in human adipose tissue physiology and systemic insulin sensitivity, possibly avoiding cellular senescence and inflammation, and in consequence preserving adipose tissue adipogenesis.

Innovation

Even though the role of H_2S on adipogenesis has been previously studied in mice, no previous studies investigated the impact of H_2S on human adipose tissue. The current study demonstrates the relevance of H_2S biosynthesis in human adipogenesis and adipose tissue physiology. This study also shows the first whole proteome persulfidation analysis in human adipocytes, suggesting that persulfidation might preserve the function of those proteins involved in adipogenesis. Altogether these data point to the potentiation of adipose tissue H_2S biosynthesis as a possible therapeutic approach to improve adipose tissue dysfunction in patients with obesity and insulin resistance (Figure 1).

Comas

Material and Methods

Subjects' recruitment for adipose tissue samples

Ex vivo experiments in adipose tissue explants

Cohort 1. Paired SAT and VAT were obtained from 20 obese participants undergoing open abdominal surgery (gastrointestinal bypass) under general anesthesia after an overnight fast. Anthropometric and clinical parameters were detailed in Suppl Table 1. The study had the approval of the ethical committee, and all patients gave informed written consent.

These experiments were performed as previously described [14]. In brief, samples of adipose tissue were immediately transported to the laboratory (5–10 min). The handling of tissue was carried out under strictly aseptic conditions. The tissue was cut with scissors into small pieces (5–10 mg) and incubated in buffer plus albumin (3 ml/g of tissue) for 30 min. After incubation, the tissue explants were centrifuged for 30 s at 400*g*. Then ~100 mg of minced tissue was placed into 1 ml M199 (Life Technologies, Invitrogen) containing 10% fetal bovine serum (Hyclone, Thermo Fisher Scientific), 100 unit/ml penicillin (Life Technologies, Invitrogen), and 100 µg/ml streptomycin (Life Technologies, Invitrogen) and incubated for 16 h in suspension culture under aseptic conditions. The following treatments were performed: i) Vehicle or GYY4137 (5 µM) administration during 16 h at 37ºC to evaluate the effects of exogenous H_2S administration (N=5); and ii) Vehicle or L-cysteine (10 mM) and pyridoxal 5'-phosphate (2 mM), as an inductor of the transsulfuration pathway (H_2S-synthesising enzymes), during 16 h at 37ºC to evaluate the effects of endogenous H_2S biosynthesis (N=20). In addition, the effect of GYY4137 (200 µM, 1 h at 37ºC) in adipose tissue lysates were also tested.

Comas

Cross-sectional studies

In cohort 2, a group of 241 [122 visceral (VAT) and 119 subcutaneous (SAT) adipose tissues] from participants with normal body weight and different degrees of obesity, with body mass index (BMI) within 20 and 68 kg/m^2, were analyzed. In a third cohort of morbidly obese (BMI > 35 kg/m^2) subjects with different degrees of insulin action (measured using hyperinsulinemic-euglycemic clamp as detailed below), 35 paired SAT and VAT samples (Cohort 3) were studied. Altogether these subjects were recruited at the Endocrinology Service of the Hospital of Girona "Dr Josep Trueta". All subjects were of Caucasian origin and reported that their body weight had been stable for at least three months before the study. Subjects were studied in the post-absorptive state. BMI was calculated as weight (in kg) divided by height (in m) squared. They had no systemic disease other than obesity or type 2 diabetes, and all were free of any infections in the previous month before the study. Type 2 diabetes was diagnosed following the criteria of the Expert Committee on the Diagnosis and Classification of Diabetes (85). The characteristics of patients with type 2 diabetes are described in Suppl Table 2 and Suppl Table 3. Liver diseases (specifically tumoral disease and HCV infection) and thyroid dysfunction were specifically excluded by biochemical work-up. All subjects gave written informed consent, validated and approved by the ethical committee of the Hospital of Girona "Dr Josep Trueta", after the purpose of the study was explained to them. Samples and data from patients included in this study were provided by the FATBANK platform promoted by the CIBEROBN and coordinated by the IDIBGI Biobank (Biobanc IDIBGI, B.0000872), integrated in the Spanish National Biobanks Network and they were processed following standard operating procedures with the appropriate approval of the Ethics, External Scientific and FATBANK Internal Scientific Committees.

Interventional studies

Comas

In cohort 4, twenty-five Caucasian obese (BMI= 43.7 ± 4.6 kg/m^2, age=47 ± 9 years [mean ±SD]) subjects, who underwent bariatric surgery thought Roux-en-Y gastric bypass in Hospital of Girona "Dr Josep Trueta" were part of an ongoing study [14]. Inclusion criteria were age between 30 and 60 years, BMI ≥ 35 kg/m^2 and ability to understand the study protocol. Exclusion criteria were use of medications able to interfere with insulin action and history of a chronic systemic disease. Adipose tissue samples from the SAT depot were obtained during bariatric surgery. Postoperative samples of SAT were obtained by subcutaneous biopsy at the mesogastric level after 2 years from surgery. Fasting blood samples were obtained at the same day of the biopsy. All subjects gave written informed consent, validated and approved by the ethical committee of the Hospital of Girona "Dr Josep Trueta", after the purpose of the study was explained to them.

In cohorts 5 and 6, SAT gene expression was analyzed before and 6 months after a multimodal weight reduction program consisting of a -800kcal calorie restricted diet combined with a structured (twice a week for 60min) exercise program (cohort 5, n=15; mean age: 46.2±2.5years, mean BMI: 34.5±1.8kg/m², no type 2 diabetes, no concomitant medication) and before and 12 months after bariatric surgery (cohort 6, n=32), as previously described [15]. All study protocols have been approved by the ethics committee of the University of Leipzig. All participants gave written informed consent before taking part in the study.

Adipose tissue samples were obtained from SAT and VAT depots during elective surgical procedures (cholecystectomy, surgery of abdominal hernia and gastric by-pass surgery). Both SAT and VAT samples were collected from the abdomen, following standard procedures. Samples of adipose tissue were immediately transported to the laboratory (5-10 min). The handling of tissue was carried out under strictly aseptic conditions. Adipose tissue samples were washed in PBS, cut off with forceps and scalpel into small pieces

Comas

(100 mg), and immediately flash-frozen in liquid nitrogen before stored at -80ºC. The isolation of adipocyte and stromal vascular fraction cells (SVF) was performed from 8 SAT and 8 VAT non-frozen adipose tissue samples. These samples were washed three to four times with phosphate-buffered saline (PBS) and suspended in an equal volume of PBS supplemented with 1% penicillin-streptomycin and 0.1% collagenase type I prewarmed to 37°C. The tissue was placed in a shaking water bath at 37°C with continuous agitation for 60 minutes and centrifuged for 5 minutes at 300 to 500g at room temperature. The supernatant, containing mature adipocytes, was recollected. The pellet was identified as the SVF. Isolated mature adipocytes and SVF stored at -80ºC for gene expression analysis.

Hyperinsulinemic-euglycemic clamp

Insulin action was determined by hyperinsulinemic-euglycemic clamp. After an overnight fast, two catheters were inserted into an antecubital vein, one for each arm, used to administer constant infusions of glucose and insulin and to obtain arterialized venous blood samples. A 2-h hyperinsulinemic-euglycemic clamp was initiated by a two-step primed infusion of insulin (80 mU/m^2/min for 5 min, 60 mU/m^2/min for 5 min) immediately followed by a continuous infusion of insulin at a rate of 40 mU/m^2/min (regular insulin [Actrapid; Novo Nordisk, Plainsboro, NJ]). Glucose infusion began at minute 4 at an initial perfusion rate of 2 mg/kg/min being then adjusted to maintain plasma glucose concentration at 88.3–99.1 mg/dL. Blood samples were collected every 5 min for determination of plasma glucose and insulin. Insulin sensitivity was assessed as the mean glucose infusion rate during the last 40 min. In the stationary equilibrium, the amount of glucose administered (*M*) equals the glucose taken by the body tissues and is a measure of overall insulin sensitivity.

Analytical methods

Comas

Serum glucose concentrations were measured in duplicate by the glucose oxidase method using a Beckman glucose analyser II (Beckman Instruments, Brea, California). Glycosylated haemoglobin (HbA1c) was measured by the high-performance liquid chromatography method (Bio-Rad, Muenchen, Germany, and autoanalyser Jokoh HS-10, respectively). Intra- and inter-assay coefficients of variation were less than 4% for all these tests. Serum insulin was measured in duplicate by RIA (Medgenix Diagnostics, Fleunes, Belgium). The intra-assay coefficient of variation was 5.2% at a concentration of 10 mU/l and 3.4% at 130 mU/l. The interassay coefficients of variation were 6.9 and 4.5% at 14 and 89 mU/l, respectively. HOMA-IR was calculated using the following formula: [Insulin (mU/l) x Glucose mmol/l]/22.5. Roche Hitachi Cobas c711 instrument (Roche, Barcelona, Spain) was used to do HDL cholesterol and total serum triglycerides determinations. HDL cholesterol was quantified by a homogeneous enzymatic colorimetric assay through the cholesterol esterase / cholesterol oxidase / peroxidase reaction (Cobas HDLC3). Serum fasting triglycerides were measured by an enzymatic, colorimetric method with glycerol phosphate oxidase and peroxidase (Cobas TRIGL). LDL cholesterol was calculated using the Friedewald formula.

Differentiation of human pre-adipocytes

Isolated human subcutaneous preadipocytes (Zen-Bio Inc., Research Triangle Park, NC) were plated on T-75 cell culture flasks and cultured at 37 C and 5% CO2 in DMEM/nutrient mix F-12 medium (1:1, vol/vol) supplemented with 10 U/ml penicillin/streptomycin, 10% fetal bovine serum (FBS), 1% HEPES, and 1% glutamine (all from GIBCO, Invitrogen S.A, Barcelona, Spain). One week later, the isolated and expanded human sc preadipocytes were cultured (~40,000 cells/cm2) in 12-well plates with preadipocytes medium (Zen-Bio) composed of DMEM/nutrient mix F-12 medium (1:1, vol/vol), HEPES, FBS, penicillin, and streptomycin in a humidified 37 C incubator

Comas

with 5% CO2. Twenty-four hours after plating, cells were checked for complete confluence (d 0), and differentiation was induced using differentiation medium (Zen-Bio) composed of preadipocytes medium, human insulin, dexamethasone, isobutylmethylxanthine, and PPARγ agonists (rosiglitazone). After 7 day (d7), differentiation medium was replaced with fresh adipocyte medium (Zen-Bio) composed of DMEM/nutrient mix F-12 medium (1:1, vol/vol), HEPES, FBS, biotin, pantothenate, human insulin, dexamethasone, penicillin, streptomycin, and amphotericin. Negative control (nondifferentiated cell) was performed with preadipocyte medium during all differentiation process. Fourteen days after the initiation of differentiation, cells appeared rounded with large lipid droplets apparent in the cytoplasm. Cells were then considered mature adipocytes, harvested, and stored at -80ºC for RNA/protein purification. For time course experiment, Cells were harvested and stored at -80ºC for RNA/protein purification at day 0, 2, 5, 7, 9, 12 and 14. To evaluate cell integrity, lactate dehydrogenase (LDH) activity was analyzed by Cytotoxicity Detection Kit (LDH) (Cat. nº 11644793001, Roche Diagnostics SL, Barcelona, Spain) according to the manufacturer's instructions.

Treatments CTH inhibitor DL-propargylglycine (PPG, 25 and 250 μM) administration was performed during sc adipocyte differentiation. Otherwise, after adipocyte differentiation (at d 14), sc fully differentiated adipocytes were incubated with fresh medium (control) and fresh medium containing PPG (25 and 250 μM) for 48h. GYY4137 (0.1, 1 and 5 μM, a slow H_2S donor) was administrated during the last stage (from day 7 to 14) of sc adipocyte differentiation process. At the end of each experiment, cells were harvested, and pellets and supernatants were stored at -80 ºC. All *in vitro* experiments were performed in three or four independent replicates.

Short hairpin (sh) RNA-mediated knockdown of *CTH, CBS* and *MPST* gene

Comas

Gene knockdown was performed using *CTH, CBS* and *MPST*-targeted and control (scrambled) shRNA lentiviral particles (sc-78973-V, sc-60335-V, sc-75821-V and sc-108080, Santa Cruz Biotechnology, CA, USA) following the manufacturer instructions in human subcutaneous preadipocytes at 80% of cell confluence. Adipocyte differentiation started 24 h after lentiviral transfection and no antibiotic selection was performed.

Media sulfide quantification

Sulfide concentration in cultured medium was assessed as previously described (16), using a naphthalimide-based fluorescent sensor 6-Azido-2-[2-[2-(2-hydroxyethoxy)ethoxy]ethyl]benzo[de]isoquinoline-1,3-dione (L1). This probe was chemically synthesised in Institute of Computational Chemistry and Catalysis (Chemistry Department, University of Girona) as described previously (15). L1 probe (5 μM) was included and incubated in adipose tissue (16h) or adipocyte (24h) maintenance media. In each experiment, a negative control that consisted in the incubation of cell culture media plus L1 probe (5 μM) without adipose tissue explants or adipocytes was also performed. This negative control was used to subtract spontaneous H_2S production. After incubation, media were transferred to new eppendorf tubes to be homogenized, and were kept at –80ºC in the dark, until the read. Fluorescence was read in a Biotek Cytation 5 reader at λ ex = 435 nm and λ em = 550nm in duplicate and quantified with a Na_2S standard curve (0, 7.8, 15.6, 31.25, 62.5, 125, 250 and 500 μM). Media sulfide levels were normalized by total protein amount in cell lysates in *in vitro* experiments or by total adipose tissue amount in *ex vivo* experiments.

Oil red O staining

Intracellular lipid accumulation was measured by oil red O staining. For oil red O staining, cells were washed twice with PBS, fixed in 4% formaldehyde for 1 h, and stained

Comas

for 30 min with 0.2% oil red O solution in 60% isopropanol. Cells were then washed several times with water, and excess water was evaporated by placing the stained cultures at ~32°C. To determine the extent of adipose conversion, 0.2 ml of isopropanol was added to the stained culture dish. The extracted dye was immediately removed by gentle pipetting and its optical density was monitored spectrophotometrically at 500 nm using a multiwell plate reader (Model Anthos Labtec 2010 1.7 reader).

Insulin action, sirtuin and PPARγ activities

To study insulin signaling, basal- and insulin-induced Akt phosphorylation at Ser473 normalized by total Akt protein levels (^{pSer473}Akt/Akt ratio) were measured after adipocyte differentiation (at d 14). Insulin stimulus was performed with insulin (100 nM) administration during 10 min. Sirtuin deacetylase and PPARγ transcriptional activities were measured using Sirtuin Activity Assay Kit (Fluorometric) (K324-100, BioVision, CA, USA) and PPAR gamma Transcription Factor Assay Kit (ab133101, Abcam, UK), respectively, strictly following the manufacturer's instructions.

RNA expression

RNA purification, gene expression procedures and analyses were performed, as previously described [14,18]. Briefly, RNA purification was performed using RNeasy Lipid Tissue Mini Kit (QIAgen, Izasa SA, Barcelona, Spain) and the integrity was checked by Agilent Bioanalyzer (Agilent Technologies, Palo Alto, CA). Gene expression was assessed by real time PCR using a LightCycler® 480 Real-Time PCR System (Roche Diagnostics SL, Barcelona, Spain), using TaqMan® technology suitable for relative genetic expression quantification. The RT-PCR reaction was performed in a final volume of 12 µl. The cycle program consisted of an initial denaturing of 10 min at 95 °C then 40 cycles of 15 s denaturizing phase at 95 °C and 1 min annealing and extension phase at 60 °C. A threshold cycle (Ct value) was obtained for each amplification curve and then a

Comas

ΔCt was first calculated by subtracting the Ct value for human cyclophilin A (*PPIA*) RNA from the Ct value for each sample. Fold changes compared with the endogenous control were then determined by calculating $2^{-\Delta Ct}$, so that gene expression results are expressed as expression ratio relative to *PPIA* gene expression according to the manufacturer's guidelines. TaqMan® primer/probe sets (Thermo Fisher Scientific, Waltham, MA, USA) used were as follows: Peptidylprolyl isomerase A (cyclophilin A) (4333763, PPIA as endogenous control), cystathionine γ-lyase (CTH, Hs00542284_m1), cystathionine β-synthase (CBS, Hs00163925_m1), mercaptopyruvate sulfurtransferase (MPST, Hs00560401_m1), adiponectin (ADIPOQ, Hs00605917_m1), peroxisome proliferator-activated receptor gamma (PPARG, Hs00234592_m1), fatty acid synthase (FASN, Hs00188012_m1), acetyl-CoA carboxylase alpha (ACACA, Hs00167385_m1), CCAAT/enhancer binding protein alpha (CEBPA, Hs00269972_s1), solute carrier family 2 member 4 (SLC2A4, Hs00168966_m1), insulin receptor substrate 1 (IRS1, Hs00178563_m1), Leptin (LEP, Hs00174877_m1), lipopolysaccharide binding protein (LBP, Hs01084621_m1), interleukin 6 (interferon, beta 2) (IL6, Hs00985639_m1), tumor necrosis factor (TNF, Hs00174128_m1), CD68 molecule (CD68, Hs00154355_m1), BCL2-associated X protein (BAX, Hs00180269_m1), tumor protein p53 (TP53, Hs01034249_m1) and fatty acid binding protein 4, adipocyte (FABP4, Hs01086177_m1).

Protein analysis

Protein were extracted directly in radioimmnuno precipitation assay (RIPA) buffer (0.1% SDS, 0.5% sodium deoxycholate, 1% Nonidet P-40, 150mM NaCl, and 50mM Tris-HCl, pH 8.0), supplemented with protease inhibitors (1 mM phenylmethylsulfonyl fluoride). Cellular debris and lipids were eliminated by centrifugation of the solubilized samples at 13000 rpm for 10 min at 4ºC, recovering the soluble fraction. Protein concentration was

Comas

determined using the RC/DC Protein Assay (Bio-Rad Laboratories, Hercules, CA). RIPA protein extracts (25 µg) were separated by SDS-PPGE and transferred to nitrocellulose membranes by conventional procedures. Membranes were immunoblotted with anti-CTH, CBS, MPST, FASN, β-actin (sc-365382**,** sc-133154, sc-376168, sc-20140, sc-47778, Santa Cruz Biotechnology, CA, USA), ^{pSer536}NFκB (p65), NFκB (p65), ^{pSer473}Akt and Akt (Cell Signaling Technology, Inc, MA, USA). Anti-rabbit IgG and anti-mouse IgG coupled to horseradish peroxidase was used as a secondary antibody. Horseradish peroxidase activity was detected by chemiluminescence, and quantification of protein expression was performed using Scion image software.

Label-free protein quantitation by SWATH-MS acquisition and analysis

Protein samples from human preadipocyte cell cultures and differentially mature adipocytes were isolated from three biological samples. Culture medium was removed by aspiration and washed once with PBS solutions. Culture cells were incubated with a trypsin solution at 37 ºc for 5 min and collected by centrifugation at 2000 rpm for 5 min. The supernatant was collected by aspiration and cell pellet freezed to -80 ºC until used. Samples were prepared by resuspension in 1 x Cell Lysis Buffer containing 20 mM Tris-HCl (pH 7.5),150 mM NaCl, 1 mM Na_2EDTA, 1 mM EGTA, 1% Triton, 2.5 mM sodium pyrophosphate, 1 mM **ß**-glycerophosphate, 1 mM Na_3VO_4, 1 µg/ml leupeptin, 0.5 mM PMSF, 1x protease inhibitor cocktail (Roche), at a ratio of 1 ml of buffer per 100 mg of tissue. Cells were vortexed and incubated 25 min at 4 ºC (on ice) and sonicated 4 times in a sonicator bath for 10 s. The extract was centrifugated at 14000 g at 4ºC for 15 min and supernatant used as protein source. 1 mg of protein per sample were TCA/acetone precipitated, resuspended in 50 mM TRIS-HCl, pH 8.0 containing 2.5% SDS, 1x protease inhibitor (Roche) and submitted to the tag-switch labelling for persulfidation protein enrichment as described (5). After elution from the streptavidin-beads proteins were

Comas

precipitated by TCA/acetone procedure. Precipitated samples were resuspended in 50 mM ammonium bicarbonate with 0.2 % Rapigest (Waters) for protein determination. 50 µg of protein were alkylated and trypsin-digested as previously described (27, 76), and the SWATH-MS analyses were performed at the Proteomic Facility of the Institute of Plant Biochemistry and Photosynthesis, Seville, Spain. A data-dependent acquisition (DDA) approach using nano-LC-MS/MS was first performed to generate the SWATH-MS spectral library as described by García *et al.* (27).

The peptide and protein identifications were performed using Protein Pilot software (version 5.0.1, Sciex) with the Paragon algorithm. The search was conducted against a Uniprot proteome database ID: UP000005640 (March 2019), specifying iodoacetamide with other possible Cys modifications. The false discovery rate (FDR) was set to 0.01 for both peptides and proteins. The MS/MS spectra of the identified peptides were then used to generate the spectral library for SWATH peak extraction using the add-in for PeakView Software (version 2.1, Sciex) MS/MSALL with SWATH Acquisition MicroApp (version 2.0, Sciex). Peptides with a confidence score above 99 % (as obtained from the Protein Pilot database search) were included in the spectral library.

For relative quantitation using SWATH analysis, the same samples used to generate the spectral library were analyzed using a data-independent acquisition (DIA) method. Each sample (2 µL) was analyzed using the LC-MS equipment and LC gradient described above to build the spectral library but instead used the SWATH-MS acquisition method. The method consisted of repeating an acquisition cycle of TOF MS/MS scans (230 to 1500 m/z, 60 ms acquisition time) of 60 overlapping sequential precursor isolation windows of variable width (1 m/z overlap) covering the 400 to 1250 m/z mass range with a previous TOF MS scan (400 to 1250 m/z, 50 ms acquisition time) for each cycle. The total cycle time was 3.7 s.

Comas

The targeted data extraction of the fragment ion chromatogram traces from the SWATH runs was performed by PeakView (version 2.1) with the MS/MSALL with SWATH Acquisition MicroApp (version 2.0). This application processed the data using the spectral library created from the shotgun data. Up to 10 peptides per protein and 7 fragments per peptide were selected, based on signal intensity. Any shared and modified peptides were excluded from the processing. Windows of 12 min and 20 ppm width were used to extract the ion chromatograms. SWATH quantitation was attempted for all proteins in the ion library that were identified by Protein Pilot with an FDR below 1 %. The extracted ion chromatograms were then generated for each selected fragment ion. The peak areas for the peptides were obtained by summing the peak areas from the corresponding fragment ions. PeakView computed an FDR and a score for each assigned peptide according to the chromatographic and spectra components. Only peptides with an FDR below 5% were used for protein quantitation. Protein quantitation was calculated by adding the peak areas of the corresponding peptides. To test for differential protein abundance between the two groups, MarkerView (version 1.2.1, Sciex) was used for signal normalization.

The mass spectrometry proteomics data have been deposited in the ProteomeXchange Consortium via the PRIDE (75) partner repository with identifier PXD018720.

Statistical analyses

Statistical analyses were performed using SPSS 12.0 software. The relation between variables was analyzed by simple correlation (Pearson's test and Spearman's test) and multiple regression analyses in a stepwise manner. One factor ANOVA with post-hoc Bonferroni test, paired t-test and unpaired t-test were used to compare *CTH, CBS* and *MPST* gene expression in human cohorts and *ex vivo* experiment. Nonparametric test

Comas

(Mann Whitney test) was used to analyse *in vitro* experiments. Levels of statistical significance were set at $p<0.05$.

Electronic laboratory notebook was not used.

ACKNOWLEDGEMENTS

We acknowledge the technical support in L1 synthesis of Xavier Ribas (UdG) and Miquel Costas (UdG). We want to particularly acknowledge the patients, the FATBANK platform promoted by the CIBEROBN and the IDIBGI Biobank (Biobanc IDIBGI, B.0000872), integrated in the Spanish National Biobanks Network, for their collaboration and coordination.

Author contributions: FC participated in this study conducting experiments, acquiring and analyzing data; JL, FO, MAR, MK, AL, CG and LCR participated in this study acquiring and analyzing data; WR, MB and LCR contributed to the discussion and reviewed the manuscript; JMFR and JMMN contributed to research study design, conducting experiments, analyzing and writing the manuscript.

Author Disclosure: The authors have nothing to disclose.

Funding statements: This work was partially supported by research grants PI15/01934, PI16/01173 and PI19/01712 from the Instituto de Salud Carlos III from Spain and VII Spanish Diabetes Association grants to Basic Diabetes Research Projects led by young researchers, CIBEROBN Fisiopatología de la Obesidad y Nutrición is an initiative from the Instituto de Salud Carlos III and Fondo Europeo de Desarrollo Regional (FEDER) from Spain. This work was also supported in part by FEDER through the Agencia Estatal de Investigación grant BIO2016-76633-P.

Data availability: All data generated or analyzed during this study are included in the published article (and its online supplementary files). The datasets generated during

Comas

and/or analyzed during the current study are available in the ProteomeXchange Consortium via the PRIDE with identifier PXD018720.

Supplementary files: 4 Suppl tables and 8 Suppl figures.

Comas

References

1. Acín-Pérez R, Iborra S, Martí-Mateos Y, Cook ECL, Conde-Garrosa R, Petcherski A, Muñoz M [a]M, Martínez de Mena R, Krishnan KC, Jiménez C, Bolaños JP, Laakso M, Lusis AJ, Shirihai OS, Sancho D, and Enríquez JA. Fgr kinase is required for proinflammatory macrophage activation during diet-induced obesity. *Nat Metab* 2: 974–988, 2020.

2. Akl MG, Fawzy E, Deif M, Farouk A, and Elshorbagy AK. Perturbed adipose tissue hydrogen peroxide metabolism in centrally obese men: Association with insulin resistance. *PLoS One* 12, 2017.

3. Albert JS, Yerges-Armstrong LM, Horenstein RB, Pollin TI, Sreenivasan UT, Chai S, Blaner WS, Snitker S, O'Connell JR, Gong D-W, Breyer RJ, Ryan AS, McLenithan JC, Shuldiner AR, Sztalryd C, and Damcott CM. Null Mutation in Hormone-Sensitive Lipase Gene and Risk of Type 2 Diabetes. *N Engl J Med* 370: 2307–2315, 2014.

4. Arner E, Westermark PO, Spalding KL, Britton T, Rydén M, Frisén J, Bernard S, and Arner P. Adipocyte turnover: Relevance to human adipose tissue morphology. *Diabetes* 59: 105–109, 2010.

5. Aroca A, Benito JM, Gotor C, and Romero LC. Persulfidation proteome reveals the regulation of protein function by hydrogen sulfide in diverse biological processes in Arabidopsis. *J Exp Bot* 68: 4915–4927, 2017.

6. Aroca A, Gotor C, and Romero LC. Hydrogen sulfide signaling in plants: emerging roles of protein persulfidation. *Front Plant Sci* 9, 2018.

7. Asimakopoulou A, Panopoulos P, Chasapis CT, Coletta C, Zhou Z, Cirino G, Giannis A, Szabo C, Spyroulias GA, and Papapetropoulos A. Selectivity of commonly used pharmacological inhibitors for cystathionine β synthase (CBS) and cystathionine γ lyase (CSE). *Br J Pharmacol* 169: 922–932, 2013.

8. Benavides GA, Squadrito GL, Mills RW, Patel HD, Isbell TS, Patel RP, Darley-Usmar VM, Doeller JE, and Kraus DW. Hydrogen sulfide mediates the vasoactivity of garlic. *Proc Natl Acad Sci U S A* 104: 17977–17982, 2007.

9. Cai J, Shi X, Wang H, Fan J, Feng Y, Lin X, Yang J, Cui Q, Tang C, Xu G, and Geng B. Cystathionine γ lyase–hydrogen sulfide increases peroxisome proliferator-activated receptor γ activity by sulfhydration at C139 site thereby promoting glucose uptake and lipid storage in adipocytes. *Biochim Biophys Acta - Mol Cell Biol Lipids* 1861: 419–429, 2016.

10. Carobbio S, Pellegrinelli V, and Vidal-Puig A. Adipose tissue function and expandability as determinants of lipotoxicity and the metabolic syndrome. *Adv Exp Med Biol.* 960: 161–196, 2017.

11. Chakaroun R, Raschpichler M, Klöting N, Oberbach A, Flehmig G, Kern M, Schön MR, Shang E, Lohmann T, Dreßler M, Fasshauer M, Stumvoll M, and Blüher M. Effects of weight loss and exercise on chemerin serum concentrations and adipose tissue expression in human obesity. *Metabolism* 61: 706–714, 2012.

12. Chalkiadaki A and Guarente L. High-fat diet triggers inflammation-induced cleavage of SIRT1 in adipose tissue to promote metabolic dysfunction. *Cell Metab* 16: 180–188, 2012.

13. Chattopadhyay M, Khemka VK, Chatterjee G, Ganguly A, Mukhopadhyay S, and

Chakrabarti S. Enhanced ROS production and oxidative damage in subcutaneous white adipose tissue mitochondria in obese and type 2 diabetes subjects. *Mol Cell Biochem* 399: 95–103, 2015.

14. Cheng X, Xi QY, Wei S, Wu D, Ye RS, Chen T, Qi QE, Jiang QY, Wang SB, Wang LN, Zhu XT, and Zhang YL. Critical role of miR-125b in lipogenesis by targeting stearoyl-CoA desaturase-1 (SCD-1). *J Anim Sci* 94: 65–76, 2016.

15. Choi SA, Park CS, Kwon OS, Giong HK, Lee JS, Ha TH, and Lee CS. Structural effects of naphthalimide-based fluorescent sensor for hydrogen sulfide and imaging in live zebrafish. *Sci Rep* 6: 26203–26203, 2016.

16. Comas F, Latorre J, Cussó O, Ortega F, Lluch A, Sabater M, Castells-Nobau A, Ricart W, Ribas X, Costas M, Fernández-Real JMJM, and Moreno-Navarrete JMJM. Hydrogen sulfide impacts on inflammation-induced adipocyte dysfunction. *Food Chem Toxicol* 131: 110543, 2019.

17. Comas F, Latorre J, Ortega F, Arnoriaga Rodríguez M, Lluch A, Sabater M, Rius F, Ribas X, Costas M, Ricart W, Lecube A, Fernández-Real JM, and Moreno-Navarrete JM. Morbidly obese subjects show increased serum sulfide in proportion to fat mass. *Int J Obes*, 2020.

18. Comas F, Latorre J, Ortega F, Oliveras-Cañellas N, Lluch A, Ricart W, Fernández-Real JM, Moreno-Navarrete JM, Oliveres N, Lluch A, Ricart W, Fernández-Real JM, and Moreno-Navarrete JM. Permanent cystathionine-β-Synthase gene knockdown promotes inflammation and oxidative stress in immortalized human adipose-derived mesenchymal stem cells, enhancing their adipogenic capacity. *Redox Biol*: 101668, 2020.

19. Cui Y, Liu Z, Sun X, Hou X, Qu B, Zhao F, Gao X, Sun Z, and Li Q. Thyroid hormone responsive protein spot 14 enhances lipogenesis in bovine mammary epithelial cells. *Vitr Cell Dev Biol - Anim* 51: 586–594, 2015.

20. Das A, Huang GX, Bonkowski MS, Longchamp A, Li C, Schultz MB, Kim LJ, Osborne B, Joshi S, Lu Y, Treviño-Villarreal JH, Kang MJ, Hung T tyng, Lee B, Williams EO, Igarashi M, Mitchell JR, Wu LE, Turner N, Arany Z, Guarente L, and Sinclair DA. Impairment of an Endothelial NAD+-H2S Signaling Network Is a Reversible Cause of Vascular Aging. *Cell* 173: 74–89.e20, 2018.

21. Ding Y, Wang H, Geng B, and Xu G. Sulfhydration of perilipin 1 is involved in the inhibitory effects of cystathionine gamma lyase/hydrogen sulfide on adipocyte lipolysis. *Biochem Biophys Res Commun* 521: 786–790, 2020.

22. Dóka, Ida T, Dagnell M, Abiko Y, Luong NC, Balog N, Takata T, Espinosa B, Nishimura A, Cheng Q, Funato Y, Miki H, Fukuto JM, Prigge JR, Schmidt EE, Arnér ESJ, Kumagai Y, Akaike T, and Nagy P. Control of protein function through oxidation and reduction of persulfidated states. *Sci Adv* 6: eaax8358, 2020.

23. Du J, Huang Y, Yan H, Zhang Q, Zhao M, Zhu M, Liu J, Chen SX, Bu D, Tang C, and Jin H. Hydrogen sulfide suppresses oxidized low-density lipoprotein (Ox-LDL)-stimulated monocyte chemoattractant protein 1 generation from macrophages via the nuclear factor κb (NF-κB) pathway. *J Biol Chem* 289: 9741–9753, 2014.

24. Elrayess MA, Almuraikhy S, Kafienah W, Al-Menhali A, Al-Khelaifi F, Bashah M, Zarkovic K, Zarkovic N, Waeg G, Alsayrafi M, and Jaganjac M. 4-hydroxynonenal causes impairment of human subcutaneous adipogenesis and induction of adipocyte insulin resistance. *Free Radic Biol Med* 104: 129–137, 2017.

Comas

25. Filipovic MR. Persulfidation (S-sulfhydration) and H2S. *Handb Exp Pharmacol* 230: 29–59, 2015.

26. Fu L, Liu K, He J, Tian C, Yu X, and Yang J. Direct Proteomic Mapping of Cysteine Persulfidation. *Antioxidants Redox Signal* 33: 1061–1076, 2020.

27. García I, Arenas-Alfonseca L, Moreno I, Gotor C, and Romero LC. HCN regulates cellular processes through posttranslational modification of proteins by s-cyanylation. *Plant Physiol* 179: 107–123, 2019.

28. Geng B, Cai B, Liao F, Zheng Y, Zeng Q, Fan X, Gong Y, Yang J, Cui Q hua, Tang C, and Xu G heng. Increase or Decrease Hydrogen Sulfide Exert Opposite Lipolysis, but Reduce Global Insulin Resistance in High Fatty Diet Induced Obese Mice. *PLoS One* 8: e73892–e73892, 2013.

29. Gillum MP, Kotas ME, Erion DM, Kursawe R, Chatterjee P, Nead KT, Muise ES, Hsiao JJ, Frederick DW, Yonemitsu S, Banks AS, Qiang L, Bhanot S, Olefsky JM, Sears DD, Caprio S, and Shulman GI. SirT1 regulates adipose tissue inflammation. *Diabetes* 60: 3235–3245, 2011.

30. Gupta S and Kruger WD. Cystathionine beta-synthase deficiency causes fat loss in mice. *PLoS One* 6: e27598–e27598, 2011.

31. Gustafson B, Hedjazifar S, Gogg S, Hammarstedt A, and Smith U. Insulin resistance and impaired adipogenesis. *Trends Endocrinol Metab* 26: 193–200, 2015.

32. Hine C, Harputlugil E, Zhang Y, Ruckenstuhl C, Lee BC, Brace L, Longchamp A, Treviño-Villarreal JH, Mejia P, Ozaki CK, Wang R, Gladyshev VN, Madeo F, Mair WB, and Mitchell JR. Endogenous hydrogen sulfide production is essential for dietary restriction benefits. *Cell* 160: 132–144, 2015.

33. Kahn CR, Wang G, and Lee KY. Altered adipose tissue and adipocyte function in the pathogenesis of metabolic syndrome. *J Clin Invest* 129: 3990–4000, 2019.

34. Kamoun P. Endogenous production of hydrogen sulfide in mammals. *Amino Acids* 26: 243–254, 2004.

35. Katsouda A, Szabo C, and Papapetropoulos A. Reduced adipose tissue H2S in obesity. *Pharmacol Res* 128: 190–199, 2018.

36. Khanahmadi M, Manafi B, Tayebinia H, Karimi J, and Khodadadi I. Downregulation of sirt1 is correlated to upregulation of p53 and increased apoptosis in epicardial adipose tissue of patients with coronary artery disease. *EXCLI J* 19: 1387–1398, 2020.

37. Krstic J, Reinisch I, Schupp M, Schulz TJ, and Prokesch A. P53 functions in adipose tissue metabolism and homeostasis. *Int J Mol Sci* 19, 2018.

38. Kruger WD. Cystathionine β-synthase deficiency: Of mice and men. *Mol Genet Metab* 121: 199–205, 2017.

39. Kuo MM, Kim DH, Jandu S, Bergman Y, Tan S, Wang H, Pandey DR, Abraham TP, Shoukas AA, Berkowitz DE, and Santhanam L. MPST but not CSE is the primary regulator of hydrogen sulfide production and function in the coronary artery. *Am J Physiol - Hear Circ Physiol* 310: H71–H79, 2016.

40. Kursawe R, Narayan D, Cali AMG, Shaw M, Pierpont B, Shulman GI, and Caprio S. Downregulation of ADIPOQ and PPARγ2 gene expression in subcutaneous adipose tissue

of obese adolescents with hepatic steatosis. *Obesity* 18: 1911–1917, 2010.

41. Lee ZW, Zhou J, Chen CS, Zhao Y, Tan CH, Li L, Moore PK, and Deng LW. The slow-releasing Hydrogen Sulfide donor, GYY4137, exhibits novel anti-cancer effects in vitro and in vivo. *PLoS One* 6, 2011.

42. Levert KL, Waldrop GL, and Stephens JM. A biotin analog inhibits acetyl-CoA carboxylase activity and adipogenesis. *J Biol Chem* 277: 16347–16350, 2002.

43. Liu T, Ma X, Ouyang T, Chen H, Lin J, Liu J, Xiao Y, Yu J, and Huang Y. SIRT1 reverses senescence via enhancing autophagy and attenuates oxidative stress-induced apoptosis through promoting p53 degradation. *Int J Biol Macromol* 117: 225–234, 2018.

44. Liu Z, Wu KKL, Jiang X, Xu A, and Cheng KKY. The role of adipose tissue senescence in obesityand ageing-related metabolic disorders. *Clin Sci* 134: 315–330, 2020.

45. Longo M, Zatterale F, Naderi J, Parrillo L, Formisano P, Raciti GA, Beguinot F, and Miele C. Adipose tissue dysfunction as determinant of obesity-associated metabolic complications. *Int J Mol Sci* 20, 2019.

46. Lyu Y, Su X, Deng J, Liu S, Zou L, Zhao X, Wei S, Geng B, and Xu G. Defective differentiation of adipose precursor cells from lipodystrophic mice lacking perilipin 1. *PLoS One* 10, 2015.

47. Mani S, Yang G, and Wang R. A critical life-supporting role for cystathionine γ-lyase in the absence of dietary cysteine supply. *Free Radic Biol Med* 50: 1280–1287, 2011.

48. Manna P and Jain SK. Hydrogen sulfide and L-cysteine increase phosphatidylinositol 3,4,5-trisphosphate (PIP3) and glucose utilization by inhibiting phosphatase and tensin homolog (PTEN) protein and activating phosphoinositide 3-kinase (PI3K)/serine/threonine protein kinase (A. *J Biol Chem* 286: 39848–39859, 2011.

49. Manna P and Jain SK. Vitamin D up-regulates glucose transporter 4 (GLUT4) translocation and glucose utilization mediated by cystathionine-γ-lyase (CSE) activation and H2S formation in 3T3L1 adipocytes. *J Biol Chem* 287: 42324–32, 2012.

50. Masschelin PM, Cox AR, Chernis N, and Hartig SM. The Impact of Oxidative Stress on Adipose Tissue Energy Balance. *Front Physiol* 10, 2020.

51. Miller DL and Roth MB. Hydrogen sulfide increases thermotolerance and lifespan in Caenorhabditis elegans. *Proc Natl Acad Sci U S A* 104: 20618–20622, 2007.

52. Minamino T, Orimo M, Shimizu I, Kunieda T, Yokoyama M, Ito T, Nojima A, Nabetani A, Oike Y, Matsubara H, Ishikawa F, and Komuro I. A crucial role for adipose tissue p53 in the regulation of insulin resistance. *Nat Med* 15: 1082–1087, 2009.

53. Moreno-Navarrete JM, Escoté X, Ortega F, Serino M, Campbell M, Michalski M-CC, Laville M, Xifra G, Luche E, Domingo P, Sabater M, Pardo G, Waget A, Salvador J, Giralt M, Rodriguez-Hermosa JI, Camps M, Kolditz CI, Viguerie N, Galitzky J, Decaunes P, Ricart W, Frühbeck G, Villarroya F, Mingrone G, Langin D, Zorzano A, Vidal H, Vendrell J, Burcelin R, Vidal-Puig A, and Fernández-Real JM. A role for adipocyte-derived lipopolysaccharide-binding protein in inflammation- and obesity-associated adipose tissue dysfunction. *Diabetologia* 56: 2524–2537, 2013.

54. Moreno-Navarrete JM, Ortega F, Serrano M, Rodriguez-Hermosa JI, Ricart W, Mingrone G, and Fernández-Real JM. CIDEC/FSP27 and PLIN1 gene expression run in parallel to mitochondrial genes in human adipose tissue, both increasing after weight loss. *Int J Obes*

38: 865–872, 2014.

55. Morley TS, Xia JY, and Scherer PE. Selective enhancement of insulin sensitivity in the mature adipocyte is sufficient for systemic metabolic improvements. *Nat Commun* 6: 7906, 2015.

56. Nagahara N, Nirasawa T, Yoshii T, and Niimura Y. Is novel signal transducer sulfur oxide involved in the redox cycle of persulfide at the catalytic site cysteine in a stable reaction intermediate of mercaptopyruvate sulfurtransferase? *Antioxidants Redox Signal* 16: 747–753, 2012.

57. Ortega FJ, Mercader JM, Moreno-Navarrete JM, Nonell L, Puigdecanet E, Rodriquez-Hermosa JI, Rovira O, Xifra G, Guerra E, Moreno M, Mayas D, Moreno-Castellanos N, Fernández-Formoso JA, Ricart W, Tinahones FJ, Torrents D, Malagón MM, and Fernández-Real JM. Surgery-induced weight loss is associated with the downregulation of genes targeted by MicroRNAs in adipose tissue. *J Clin Endocrinol Metab* 100: E1467–E1476, 2015.

58. Padiya R, Khatua TN, Bagul PK, Kuncha M, and Banerjee SK. Garlic improves insulin sensitivity and associated metabolic syndromes in fructose fed rats. *Nutr Metab* 8: 53, 2011.

59. Pan Z, Wang H, Liu Y, Yu C, Zhang Y, Chen J, Wang X, and Guan Q. Involvement of CSE/ H2S in high glucose induced aberrant secretion of adipokines in 3T3-L1 adipocytes. *Lipids Health Dis* 13: 155, 2014.

60. Paul BD and Snyder SH. H 2S signalling through protein sulfhydration and beyond. *Nat Rev Mol Cell Biol* 13: 499–507, 2012.

61. Pérez-Pérez R, López JA, García-Santos E, Camafeita E, Gómez-Serrano M, Ortega-Delgado FJ, Ricart W, Fernández-Real JM, and Peral B. Uncovering suitable reference proteins for expression studies in human adipose tissue with relevance to obesity. *PLoS One* 7: e30326, 2012.

62. Politis-Barber V, Brunetta HS, Paglialunga S, Petrick HL, and Holloway GP. Long-term, high-fat feeding exacerbates short-term increases in adipose mitochondrial reactive oxygen species, without impairing mitochondrial respiration. *Am J Physiol - Endocrinol Metab* 319: E373–E387, 2020.

63. Powell CR, Dillon KM, and Matson JB. A review of hydrogen sulfide (H2S) donors: Chemistry and potential therapeutic applications. *Biochem Pharmacol* 149: 110–123, 2018.

64. Rappou E, Jukarainen S, Rinnankoski-Tuikka R, Kaye S, Heinonen S, Hakkarainen A, Lundbom J, Lundbom N, Saunavaara V, Rissanen A, Virtanen KA, Pirinen E, and Pietiläinen KH. Weight Loss Is Associated With Increased NAD^+/SIRT1 Expression But Reduced PARP Activity in White Adipose Tissue. *J Clin Endocrinol {&} Metab* 101: 1263–1273, 2016.

65. Sanokawa-Akakura R, Akakura S, and Tabibzadeh S. Replicative senescence in human fibroblasts is delayed by hydrogen sulfide in a NAMPT/SIRT1 dependent manner. *PLoS One* 11: e0164710–e0164710, 2016.

66. Schmid B, Rippmann JF, Tadayyon M, and Hamilton BS. Inhibition of fatty acid synthase prevents preadipocyte differentiation. *Biochem Biophys Res Commun* 328: 1073–1082, 2005.

67. Shearin AL, Monks BR, Seale P, and Birnbaum MJ. Lack of AKT in adipocytes causes severe lipodystrophy. *Mol Metab* 5: 472–479, 2016.

68. Shibuya N, Tanaka M, Yoshida M, Ogasawara Y, Togawa T, Ishii K, and Kimura H. 3-Mercaptopyruvate sulfurtransferase produces hydrogen sulfide and bound sulfane sulfur in the brain. *Antioxidants Redox Signal* 11: 703–714, 2009.

69. Spassov SG, Donus R, Ihle PM, Engelstaedter H, Hoetzel A, and Faller S. Hydrogen Sulfide Prevents Formation of Reactive Oxygen Species through PI3K/Akt Signaling and Limits Ventilator-Induced Lung Injury. *Oxid Med Cell Longev* 2017: 3715037, 2017.

70. Szabó C. Hydrogen sulphide and its therapeutic potential. *Nat Rev Drug Discov* 6: 917–935, 2007.

71. Tinahones FJ, Araguez LCI, Murri M, Olivera WO, Torres MDM, Barbarroja N, Huelgas RG, Malagón MM, and Bekay R El. Caspase induction and BCL2 inhibition in human adipose tissue. *Diabetes Care* 36: 513–521, 2013.

72. Trayhurn P. Hypoxia and adipose tissue function and dysfunction in obesity. *Physiol Rev* 93: 1–21, 2013.

73. Tsai CY, Peh MT, Feng W, Dymock BW, and Moore PK. Hydrogen sulfide promotes adipogenesis in 3T3L1 cells. *PLoS One* 10: e0119511–e0119511, 2015.

74. Veilleux A, Blouin K, Rhéaume C, Daris M, Marette A, and Tchernof A. Glucose transporter 4 and insulin receptor substrate-1 messenger RNA expression in omental and subcutaneous adipose tissue in women. *Metabolism* 58: 624–631, 2009.

75. Vizcaíno JA, Csordas A, del-Toro N, Dianes JA, Griss J, Lavidas I, Mayer G, Perez-Riverol Y, Reisinger F, Ternent T, Xu Q-W, Wang R, and Hermjakob H. 2016 update of the PRIDE database and its related tools. *Nucleic Acids Res* 44: D447-56, 2016.

76. Vowinckel J, Capuano F, Campbell K, Deery MJ, Lilley KS, and Ralser M. The beauty of being (label)-free: Sample preparation methods for SWATH-MS and next-generation targeted proteomics. *F1000Research* 2: 272, 2014.

77. Whiteman M, Gooding KM, Whatmore JL, Ball CI, Mawson D, Skinner K, Tooke JE, and Shore AC. Adiposity is a major determinant of plasma levels of the novel vasodilator hydrogen sulphide. *Diabetologia* 53: 1722–1726, 2010.

78. Xu C, Cai Y, Fan P, Bai B, Chen J, Deng HB, Che CM, Xu A, Vanhoutte PM, and Wang Y. Calorie restriction prevents metabolic aging caused by abnormal sirt1 function in adipose tissues. *Diabetes* 64: 1576–1590, 2015.

79. Xue R, Hao DD, Sun JP, Li WW, Zhao MM, Li XH, Chen Y, Zhu JH, Ding YJ, Liu J, and Zhu YC. Hydrogen sulfide treatment promotes glucose uptake by increasing insulin receptor sensitivity and ameliorates kidney lesions in type 2 diabetes. *Antioxidants Redox Signal* 19: 5–23, 2013.

80. Yang G, Ju Y, Fu M, Zhang Y, Pei Y, Racine M, Baath S, Merritt TJS, Wang R, and Wu L. Cystathionine gamma-lyase/hydrogen sulfide system is essential for adipogenesis and fat mass accumulation in mice. *Biochim Biophys Acta - Mol Cell Biol Lipids* 1863: 165–176, 2018.

81. Yang G, Wu L, Jiang B, Yang W, Qi J, Cao K, Meng Q, Mustafa AK, Mu W, Zhang S, Snyder SH, and Wang R. H2S as a physiologic vasorelaxant: Hypertension in mice with deletion of cystathionine γ-lyase. *Science (80-)* 322: 587–590, 2008.

Comas

82. Zhan T, Poppelreuther M, Ehehalt R, and Füllekrug J. Overexpressed FATP1, ACSVL4/FATP4 and ACSL1 Increase the Cellular Fatty Acid Uptake of 3T3-L1 Adipocytes but Are Localized on Intracellular Membranes. *PLoS One 7: e45087, 2012.*

83. Zhang D, MacInkovic I, Devarie-Baez NO, Pan J, Park CM, Carroll KS, Filipovic MR, and Xian M. Detection of protein S-sulfhydration by a tag-switch technique. *Angew Chemie - Int Ed* 53: 575–581, 2014.

84. Zivanovic J, Kouroussis E, Kohl JB, Adhikari B, Bursac B, Schott-Roux S, Petrovic D, Miljkovic JL, Thomas-Lopez D, Jung Y, Miler M, Mitchell S, Milosevic V, Gomes JE, Benhar M, Gonzales-Zorn B, Ivanovic-Burmazovic I, Torregrossa R, Mitchell JR, Whiteman M, Schwarz G, Snyder SH, Paul BD, Carroll KS, and Filipovic MR. Selective Persulfide Detection Reveals Evolutionarily Conserved Antiaging Effects of S-Sulfhydration. *Cell Metab* 30: 1152–1170.e13, 2019.

85. 2. Classification and diagnosis of diabetes. *Diabetes Care* 38: S8–S16, 2015.

Comas

Table 1. Effects of transsulfuration pathway activation (PLP+CYS administration) on adipogenic, CTH and CBS gene expression and on H_2S production in cohort 1. These data were analysed using Paired T test.

	SAT (n=20)			VAT (n=20)		
	Control	**PLP+CYS**	**p**	**Control**	**PLP+CYS**	**p**
ADIPOQ (RU)	0.482±0.22	0.875±0.45	**<0.0001**	0.505±0.23	0.867±0.46	**<0.0001**
PPARG (RU)	0.022±0.009	0.035±0.015	**<0.0001**	0.025±0.013	0.040±0.017	**<0.0001**
SLC2A4 (RU)	0.0053±0.003	0.0085±0.004	**<0.0001**	0.0076±0.004	0.0119±0.007	**<0.0001**
FASN (RU)	0.167±0.08	0.232±0.13	**0.002**	0.203±0.08	0.274±0.16	**0.006**
LEP (RU)	0.125±0.06	0.209±0.12	**<0.0001**	0.075±0.07	0.142±0.13	**<0.0001**
IRS1 (RU)	0.0022±0.001	0.0022±0.001	0.9	0.0021±0.0008	0.0022±0.001	0.3
UCP3 (RU)	0.0003±0.0001	0.0003±0.0001	0.3	0.0005±0.0002	0.0004±0.0002	0.4
CIDEA (RU)	0.039±0.02	0.065±0.04	**0.001**	0.128±0.06	0.210±0.11	**<0.0001**
SIRT1 (RU)	0.017±0.005	0.026±0.008	**<0.0001**	0.025±0.009	0.035±0.013	**0.002**
CTH (RU)	0.0009±0.0003	0.0031±0.002	**<0.0001**	0.0031±0.001	0.0072±0.003	**0.001**
CBS (RU)	0.0024±0.001	0.0051±0.003	**<0.0001**	0.0048±0.002	0.0084±0.005	**0.001**
H_2S (nmol/mg AT)	0.57±0.4	2.05±1.1	**0.002**	0.48±0.3	2.11±1.5	**0.004**

Comas

Table 2. Correlation between *CTH, CBS* and *MPST* gene expression and anthropometric and clinical characteristics and selected gene expression in SAT (n=119) and VAT (n=122) from cohort 2.

	SAT *CTH*		**SAT *CBS***		**SAT *MPST***	
	r	**p**	**r**	**p**	**r**	**p**
Age (years)	0.05	0.6	0.01	0.9	-0.13	0.1
BMI (kg/m^2)	-0.52	**<0.0001**	-0.39	**<0.0001**	-0.32	**<0.0001**
Fasting glucose (mg/dl)	-0.09	0.3	-0.18	0.06	-0.22	**0.04**
HOMA-IR (n=34)	-0.61	**<0.0001**	-0.62	**<0.0001**	0.20	0.2
Total Cholesterol (mg/dl)	0.04	0.6	-0.05	0.6	-0.03	0.7
HDL Cholesterol (mg/dl)	0.18	0.06	-0.10	0.3	-0.02	0.8
LDL Cholesterol (mg/dl)	0.07	0.4	0.05	0.5	0.01	0.8
Fasting Triglycerides (mg/dl)	-0.22	**0.03**	-0.06	0.5	-0.21	**0.04**
FASN (R.U.)	0.50	**<0.0001**	0.45	**<0.0001**	0.46	**<0.0001**
ACACA (R.U.)	0.33	**0.001**	0.27	**0.006**	-0.02	0.8
PPARG (R.U.)	0.59	**<0.0001**	0.29	**0.01**	0.10	0.3
SLC2A4 (R.U.)	0.55	**<0.0001**	0.42	**<0.0001**	0.46	**<0.0001**
IRS1 (R.U.)	0.41	**<0.0001**	0.47	**<0.0001**	0.29	**0.004**
SIRT1 (R.U.)	0.52	**<0.0001**	0.36	**0.001**	-0.03	0.7
PPARGC1A (R.U.)	0.41	**<0.0001**	0.49	**<0.0001**	0.05	0.6
LEP (R.U.)	-0.37	**0.001**	-0.33	**0.008**	-0.22	**0.04**
LBP (R.U.)	-0.46	**<0.0001**	-0.26	**0.02**	-0.06	0.6
TNF (R.U.)	0.06	0.6	-0.03	0.7	-0.36	**<0.0001**
CD68 (R.U.)	0.05	0.6	0.03	0.7	-0.18	0.1
	VAT *CTH*		**VAT *CBS***		**VAT *MPST***	
	r	**p**	**r**	**p**	**r**	**p**
Age (years)	0.07	0.4	0.11	0.2	0.20	0.1
BMI (kg/m^2)	-0.46	**<0.0001**	-0.36	**<0.0001**	-0.26	**0.01**
Fasting glucose (mg/dl)	-0.17	0.08	-0.02	0.8	0.09	0.2
HOMA-IR (n=34)	-0.11	0.5	-0.08	0.6	-0.02	0.9
Total Cholesterol (mg/dl)	0.15	0.1	0.02	0.8	0.12	0.1
HDL Cholesterol (mg/dl)	-0.01	0.9	-0.09	0.4	-0.04	0.6
LDL Cholesterol (mg/dl)	0.20	0.05	0.02	0.8	0.17	0.1
Fasting Triglycerides (mg/dl)	0.02	0.8	0.11	0.2	-0.04	0.6
FASN (R.U.)	0.41	**<0.0001**	0.32	**0.001**	0.26	**0.01**
ACACA (R.U.)	0.35	**0.001**	0.37	**<0.0001**	-0.10	0.2
PPARG (R.U.)	0.44	**<0.0001**	0.39	**<0.0001**	0.12	0.3
SLC2A4 (R.U.)	0.48	**<0.0001**	0.39	**<0.0001**	0.41	**<0.0001**
IRS1 (R.U.)	0.44	**<0.0001**	0.39	**<0.0001**	0.30	**0.003**
SIRT1 (R.U.)	0.55	**<0.0001**	0.37	**<0.0001**	-0.08	0.5
PPARGC1A (R.U.)	0.25	**0.02**	0.12	0.3	-0.09	0.3
LEP (R.U.)	-0.39	**<0.0001**	-0.38	**<0.0001**	0.20	0.1
LBP (R.U.)	-0.25	**0.02**	-0.38	**<0.0001**	-0.02	0.9
TNF (R.U.)	-0.07	0.5	-0.02	0.8	-0.29	**0.005**
CD68 (R.U.)	0.05	0.5	0.19	0.1	-0.03	0.8

VAT, visceral adipose tissue; SAT, subcutaneous adipose tissue; HOMA-IR, Homeostasis Model Assessment – Insulin Resistance Index; R.U., relative gene expression units.

Comas

Table 3. Correlation between *CTH, CBS* and *MPST* gene expression and anthropometric and clinical characteristics and selected gene expression in SAT (n=35) and VAT (n=35) from cohort 3.

	SAT *CTH*		**SAT *CBS***		**SAT *MPST***	
	r	**p**	**r**	**p**	**r**	**p**
Age (years)	0.20	0.2	0.15	0.3	-0.16	0.4
BMI (kg/m^2)	0.05	0.7	-0.19	0.2	0.12	0.5
Waist circumference (cm)	-0.19	0.2	-0.23	0.2	-0.50	**0.002**
HOMA-IR	0.31	0.06	-0.29	0.08	-0.34	0.08
M (mg/kg·min)	0.24	0.2	0.40	**0.03**	0.35	0.07
Fasting Glucose (mg/dL)	-0.01	0.9	-0.13	0.4	-0.38	0.05
Total Cholesterol (mg/dl)	0.29	0.08	0.27	0.1	0.09	0.6
HDL Cholesterol (mg/dl)	0.32	0.05	0.06	0.7	-0.23	0.2
LDL Cholesterol (mg/dl)	0.21	0.2	0.28	0.1	0.07	0.7
Fasting triglycerides (mg/dl)	0.02	0.9	-0.05	0.7	0.16	0.4
PPARG (R.U.)	0.58	**<0.0001**	-0.33	0.05	0.23	0.2
ADIPOQ (R.U.)	0.56	**<0.0001**	0.17	0.3	0.38	0.05
SLC2A4 (R.U.)	0.13	0.4	0.53	**0.001**	0.44	**0.01**
IRS1 (R.U.)	0.41	**0.01**	0.23	0.2	0.32	0.1
SIRT1 (R.U.)	0.66	**<0.0001**	0.01	0.9	-0.11	0.6
PPARGC1A (R.U.)	0.85	**<0.0001**	0.04	0.8	0.15	0.4
TNF (R.U.)	-0.36	**0.04**	0.22	0.2	0.23	0.2
BAX (R.U.)	-0.66	**0.003**	0.24	0.2	0.05	0.8
TP53 (R.U.)	-0.65	**0.004**	0.28	0.1	-0.11	0.6
	VAT *CTH*		**VAT *CBS***		**VAT *MPST***	
	r	**p**	**r**	**p**	**r**	**p**
Age (years)	-0.16	0.3	0.07	0.7	0.13	0.4
BMI (kg/m^2)	-0.06	0.7	-0.08	0.6	-0.28	0.1
Waist circumference (cm)	-0.44	**0.008**	-0.08	0.6	-0.15	0.4
HOMA-IR	-0.37	**0.02**	0.08	0.6	-0.22	0.2
M (mg/kg·min)	0.21	0.2	0.16	0.4	0.33	0.08
Fasting Glucose (mg/dL)	-0.08	0.6	0.10	0.5	0.06	0.7
Total Cholesterol (mg/dl)	0.05	0.7	0.01	0.9	-0.10	0.5
HDL Cholesterol (mg/dl)	0.14	0.4	0.21	0.2	0.22	0.2
LDL Cholesterol (mg/dl)	0.05	0.7	-0.04	0.8	-0.18	0.3
Fasting triglycerides (mg/dl)	-0.22	0.1	-0.35	**0.04**	0.02	0.9
PPARG (R.U.)	0.28	0.1	-0.29	0.1	0.46	**0.005**
ADIPOQ (R.U.)	0.41	**0.01**	-0.15	0.3	0.42	**0.01**
SLC2A4 (R.U.)	0.19	0.2	0.18	0.3	0.61	**<0.0001**
IRS1 (R.U.)	0.46	**0.005**	0.27	0.1	0.14	0.4
SIRT1 (R.U.)	0.48	**0.005**	0.19	0.3	-0.30	0.1
PPARGC1A (R.U.)	0.43	**0.01**	0.16	0.3	-0.32	0.1
TNF (R.U.)	-0.31	0.06	0.18	0.3	-0.17	0.3
BAX (R.U.)	-0.44	**0.02**	0.23	0.2	0.29	0.1
TP53 (R.U.)	-0.42	**0.03**	0.27	0.1	0.09	0.6

VAT, visceral adipose tissue; SAT, subcutaneous adipose tissue; HOMA-IR, Homeostasis Model Assessment – Insulin Resistance Index; M, systemic insulin sensitivity measured by hyperinsulinemic-euglycemic clamp; R.U., relative gene expression units.

Comas

Figure legends

Figure 1. Graphic illustration summarizing how in patients with obesity and insulin resistance adipose tissue H_2S biosynthesis is attenuated, and this attenuation results in adipose tissue dysfunction, possibly promoted by decreased persulfidation in key adipogenic proteins. This summary suggests that the potentiation of adipose tissue H_2S biosynthesis might be a possible therapeutic approach to improve obesity-associated adipose tissue dysfunction.

Figure 2. A) Effect of GYY4137 (5 µM) administration for 16h on *ADIPOQ, FASN SLC2A4* and *SIRT1* mRNA levels and on tissue culture media sulfide levels in human adipose tissue explants (Cohort1). **B-C)** GYY4137 (200 µM) effects on Sirtuin deacetylase **(B)** and PPARγ transcriptional **(C)** activity (1 h, 37ºC) in adipose tissue lysates (Cohort1). **D)** Effect of L-cysteine (10 mM) and pyridoxal 5'-phosphate (2 mM) (PLP+ Cys) administration for 16h on sulfide concentration in media (N=8) and *ADIPOQ* gene expression (N=20) in human SAT and VAT explants (Cohort1). **E-F)** Bivariate correlation (Spearman r) between *ADIPOQ*, *PPARG*, *SLC2A4, FASN, SIRT1, CTH* and *CBS* and media sulfide levels in both SAT **(E)** and VAT **(F)** in cohort 1.

Figure 3. A-D) Bivariate correlation (Spearman r) between percent change in *ADIPOQ* **(A)**, *SLC2A4* **(B)**, *FASN* **(C)** and *SIRT1* **(D)** after PLP and Cys administration and HbA1c levels in both SAT and VAT (Cohort1). **E-H)** Bivariate correlation (Spearman r) between percent change in *ADIPOQ* **(E)**, *SLC2A4* **(F)**, *FASN* **(G)** and *SIRT1* **(H)** after PLP and Cys administration and insulin sensitivity (M value) (Cohort1).

Figure 4. A-C) SAT and VAT *CTH, CBS* and *MPST* gene expression according to obesity and type 2 diabetes (Cohort 2). **p<0.01 *vs* non-obese; †p<0.05 *vs* obese participants. **D)**

Comas

Bivariate correlation (Spearman r) between CTH protein and *CTH* mRNA levels in both SAT and VAT (Cohort 2). **E-F)** Bivariate correlation between insulin sensitivity and SAT *CTH* **(E)** and *CBS* **(F)** gene expression in cohort 3. **G-I)** *CTH, MPST* and *CBS* gene expression in SAT and VAT adipose tissue cell fractions [stromal vascular cell fraction (SVF) and adipocytes] in cohort 2. *p<0.05 and **p<0.01 *vs* SVF; †p<0.05 *vs* SAT cells.

Figure 5. A-B) Basal and stimulated [treated with L-cysteine 250 µM) and pyridoxal 5'-phosphate (50 µM)] H_2S production **(A)** and stimulated/basal H_2S ratio **(B)** in human preadipocytes and fully differentiated adipocytes. **C-F)** *CTH, MPST, ADIPOQ* and *CBS* gene expression during human preadipocyte differentiation into adipocytes. Time-course experiment included day 0, 2, 5, 7, 9, 12 and 14. **G)** CTH, MPST, CBS and FASN protein levels in human preadipocytes and adipocytes. Protein levels were normalized by β-actin.

Figure 6. A-E) GYY4137 (5 µM, green boxes in preadipocytes and orange boxes in adipocytes) effects on PPARγ transcriptional and Sirtuin deacetylase activity in preadipocytes **(A,B)** and adipocytes **(C,D)**. **E)** GYY4137 (5 µM) effects on insulin-stimulated Akt phosphorylation at Ser473 in human differentiated adipocytes. *p<0.05 and **p<0.01 *vs* vehicle. †p<0.05 and ††p<0.01 *vs* basal. **F-I)** GYY4137 (0.1, 1, 5 µM) and GYY4137 (5 µM) + PPG (250 µM) on adipogenic [*ADIPOQ* **(F)**, *FABP4* **(G)**, *CEBPA* **(H)**, *SLC2A4* **(I)**] gene expression in human differentiated adipocytes. *p<0.05 and **p<0.01 *vs* vehicle.

Figure 7. A-M) Effects of DL-Propargylglycine (PPG, 25 and 250 µM) administration on intracellular lipid accumulation measured by Oil red staining (10X, OM) **(A)**, FAS protein levels **(B)**, adipogenic (*ADIPOQ, PPARG, FABP4, FASN, PLIN1*) gene expression **(C-G)**, expression of inflammatory and cellular senescence gene markers (*TNF, IL6, BAX, TP53*) **(H-K)**, LDH activity **(L)** and ^{pSer536}NFκB / ^{pSer536}NFκB ratio

Comas

measured using western blot band intensities **(M)** at day 14 of human sc adipocyte differentiation. **N)** Effects of DL-Propargylglycine (PPG 250 µM) administration on insulin-stimulated Akt phosphorylation at Ser473 in human differentiated adipocytes. *p<0.05 and **p<0.01 *vs* differentiated control cells (Diff); †<0.05 *vs* basal. To see this illustration in color, the reader is referred to the online version of this article at www.liebertpub.com/ars.

Figure 8. A-C) Effects of *CTH* **(A)**, *CBS* **(B)** and *MPST* **(C)** gene knockdown on H_2S-synthesising enzymes (*CTH, CBS, MPST*)-, adipogenic (*ADIPOQ, FABP4, FASN, PPARG, CEBPA*)-, insulin pathway (*SLC2A4, IRS1*)- and inflammatory (*IL6,* TNF)-related gene expression at day 14 of human subcutaneous adipocyte differentiation. *p<0.05, **p<0.01 and ***p<0.001 *vs* shC differentiated control cells.

Figure 9. A-B) Representation of protein persulfidation-enriched biological processes **(A)** and KEGG pathways **(B)** in human adipocytes. **C)** Persulfidation ratio of proteins involved in adipocyte lipid metabolism and control proteins (ACTB, ENO1, PARK7). Level of protein persulfidation in preadipocyte (clear grey boxes) compared to the level in adipocyte (dark grey boxes). ACACA, Acetyl-CoA carboxylase 1; ACSL1, Long-chain-fatty-acid--CoA ligase 1; FABP4, Fatty acid-binding protein; FASN, Fatty acid synthase; LIPE, Hormone-sensitive lipase; PLIN1, Perilipin-1; PLIN4, Perilipin-4; SLC2A4, Solute carrier family 2 member 4; THRSP, Thyroid hormone-inducible hepatic protein; ACTB, β-actin; ENO1, enolase 1; PARK7, Parkinsonism associated deglycase.

Figure 1

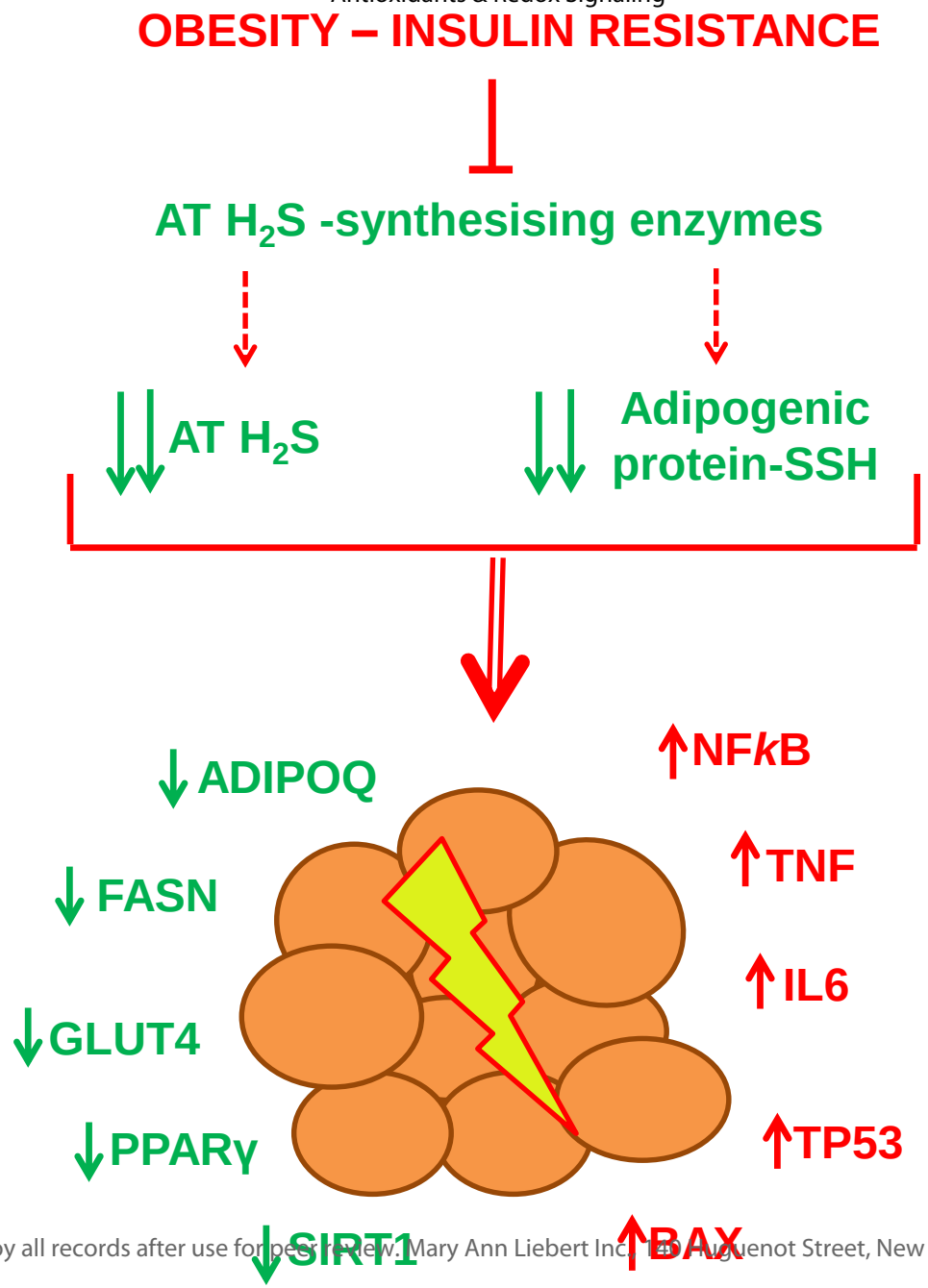

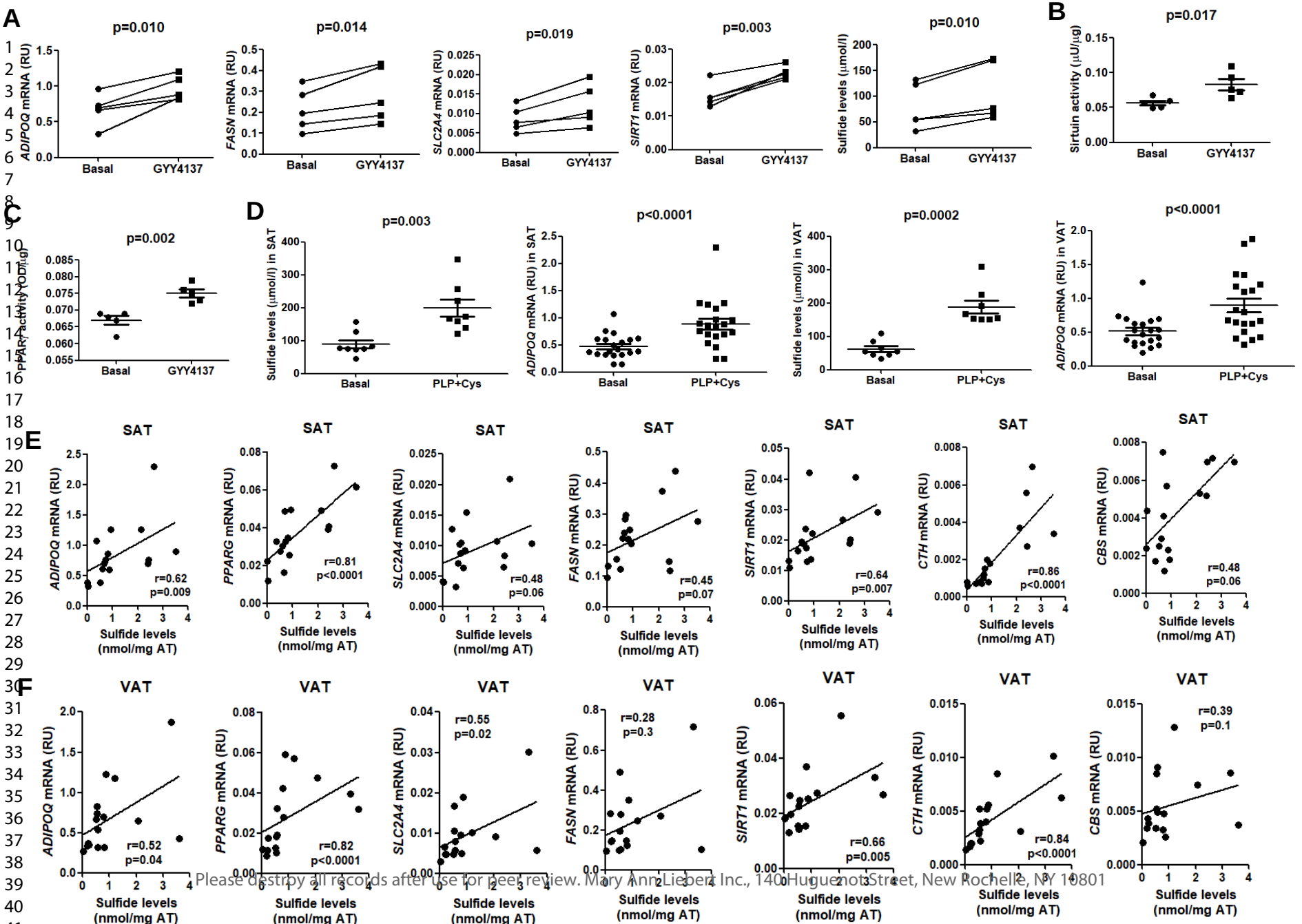

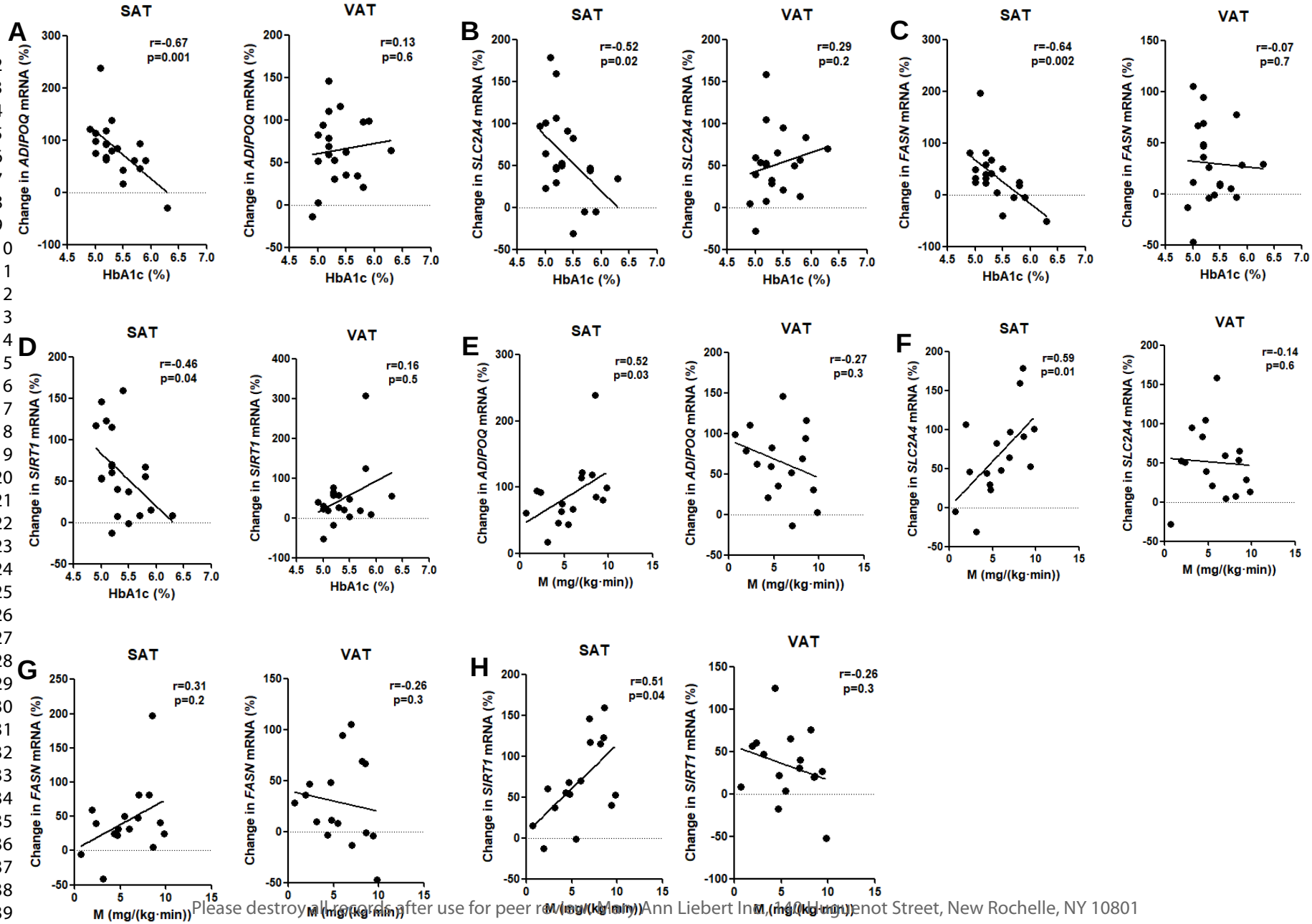

Figure 4

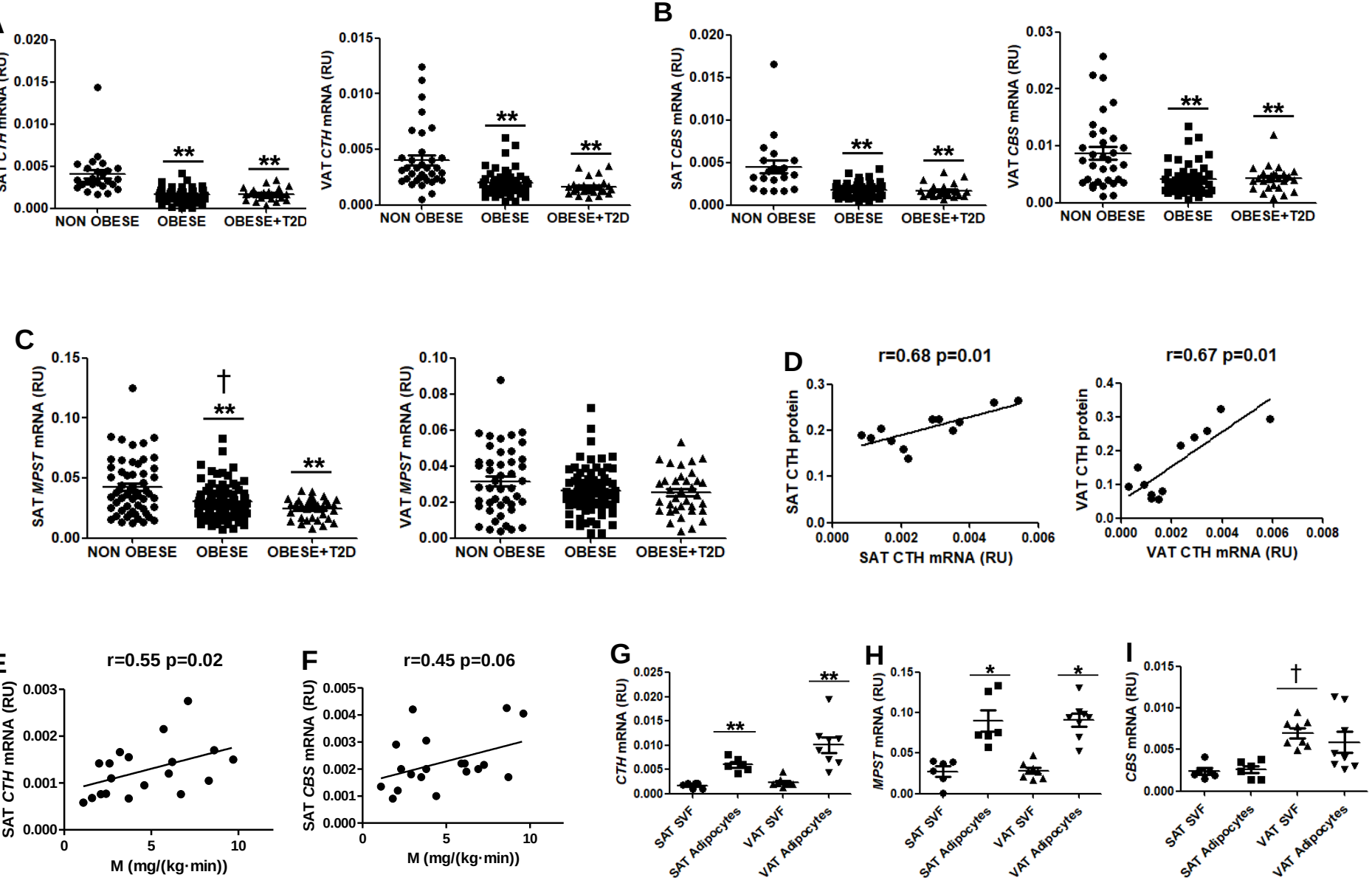

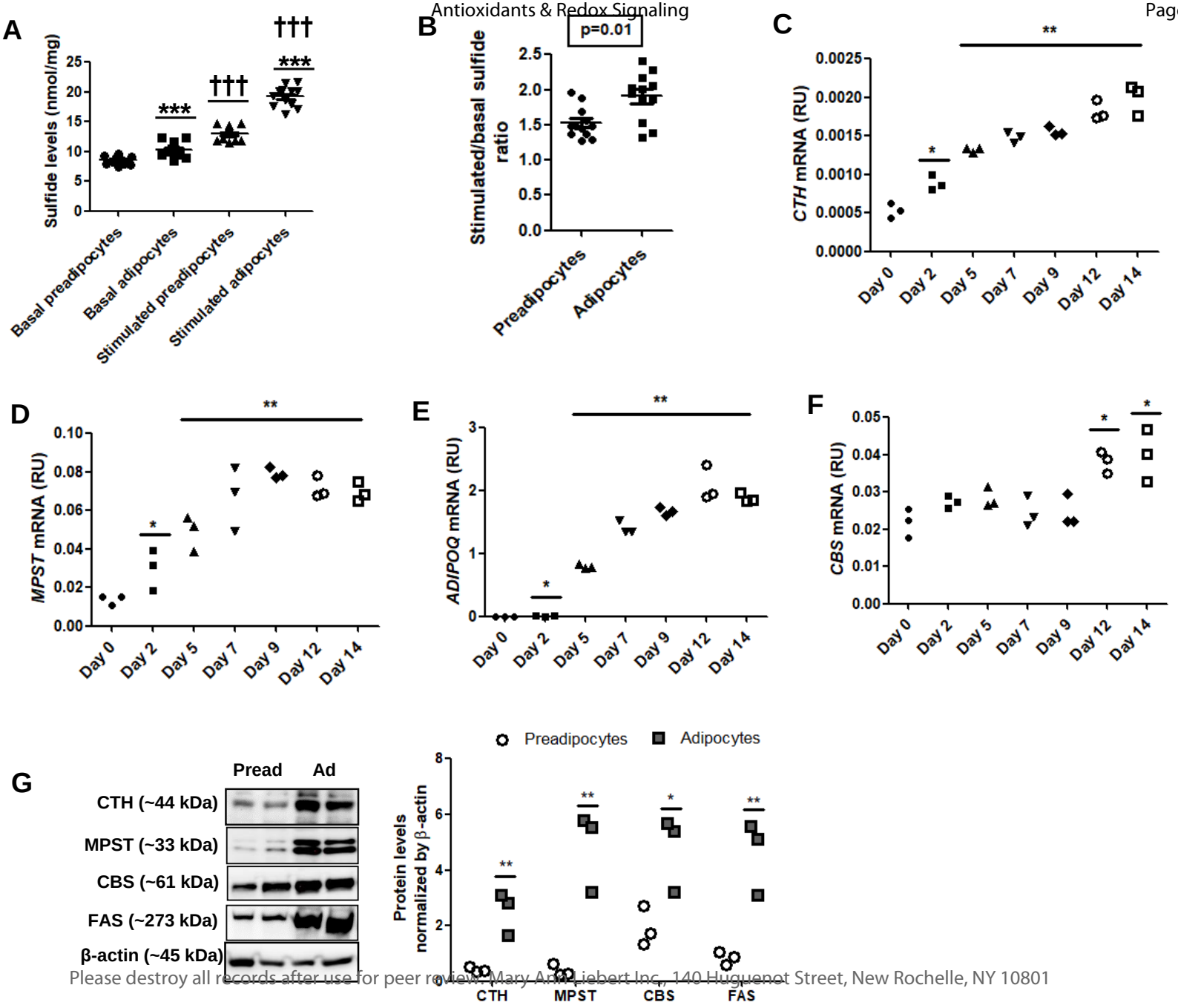

Figure 6

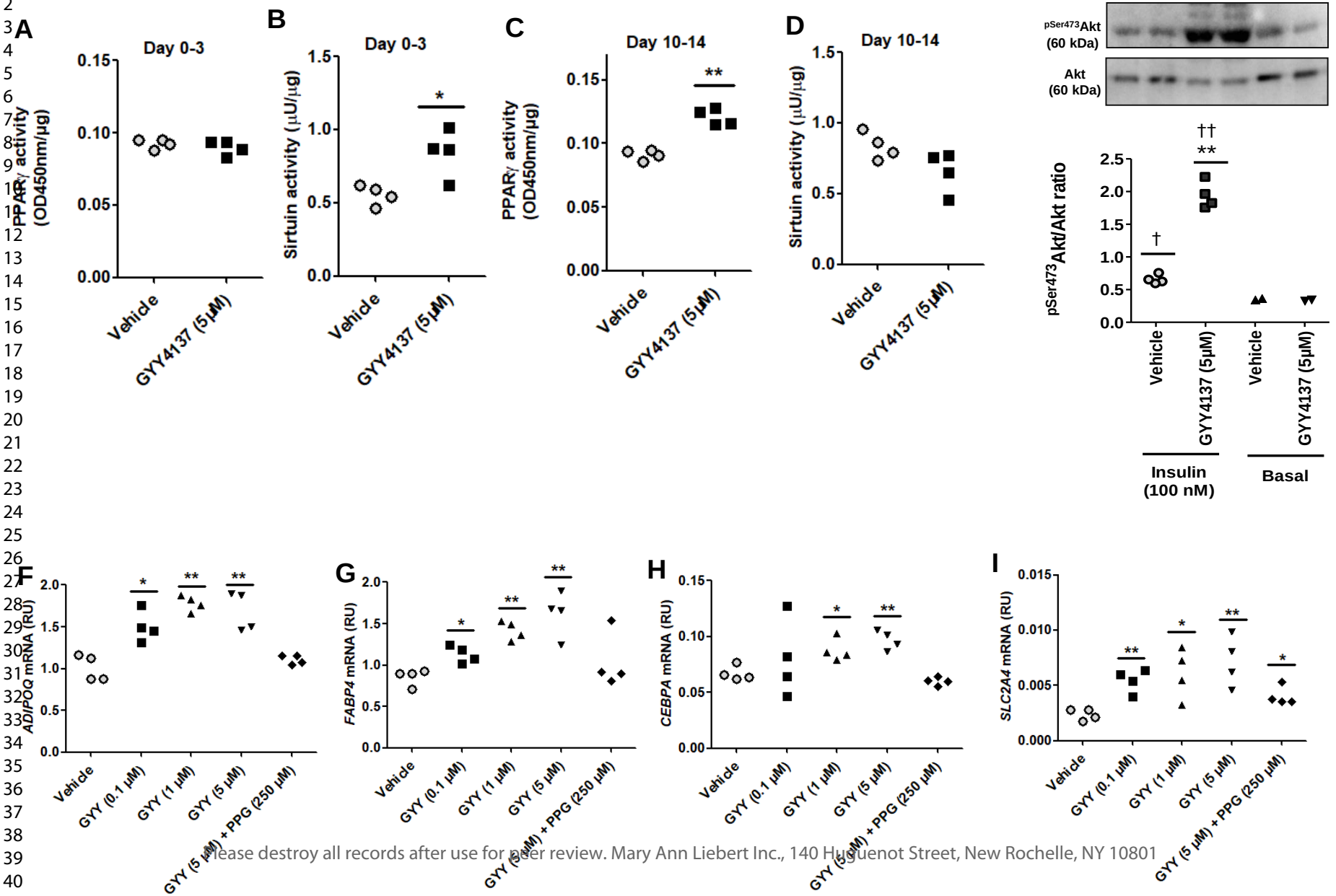

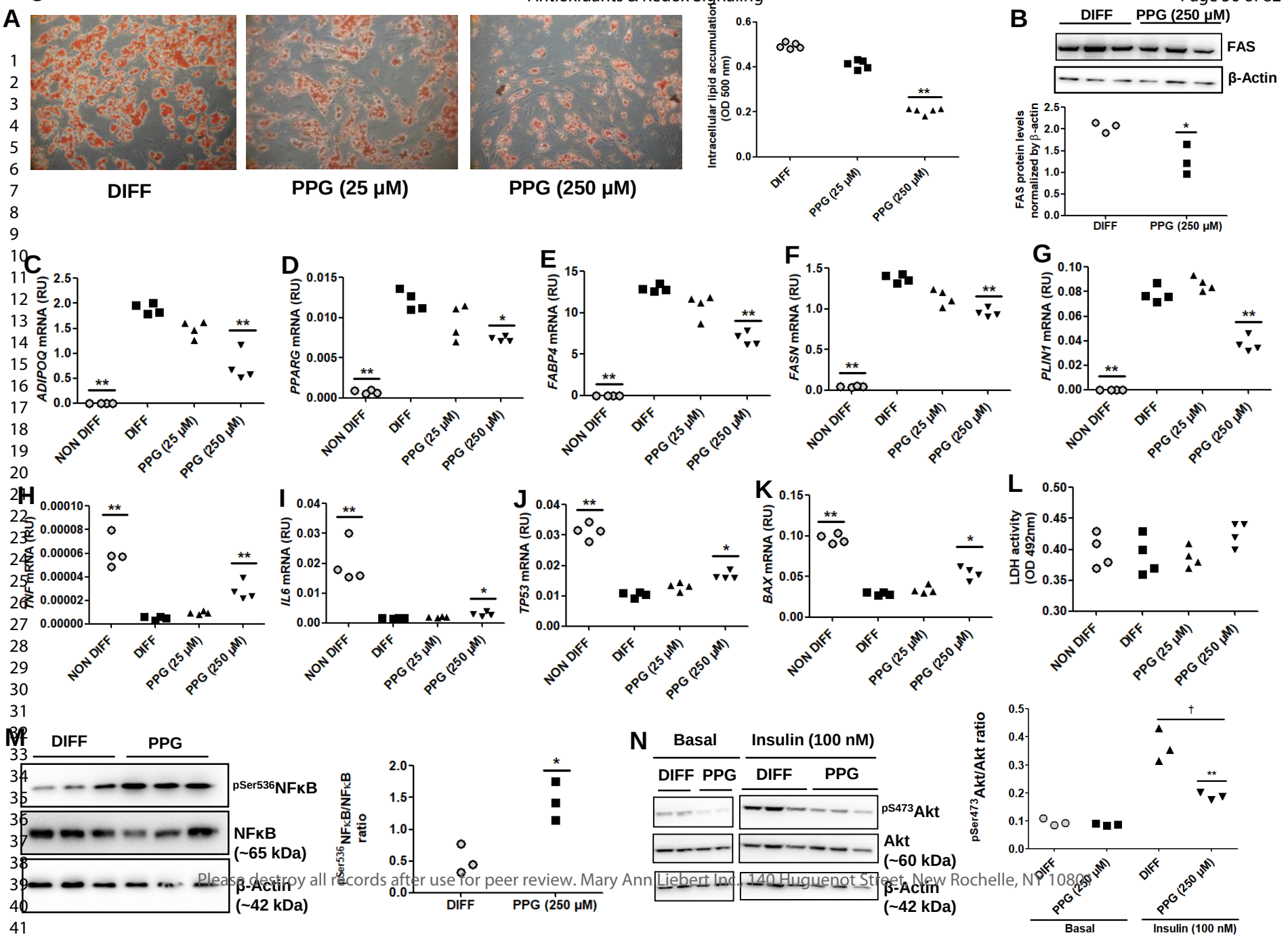

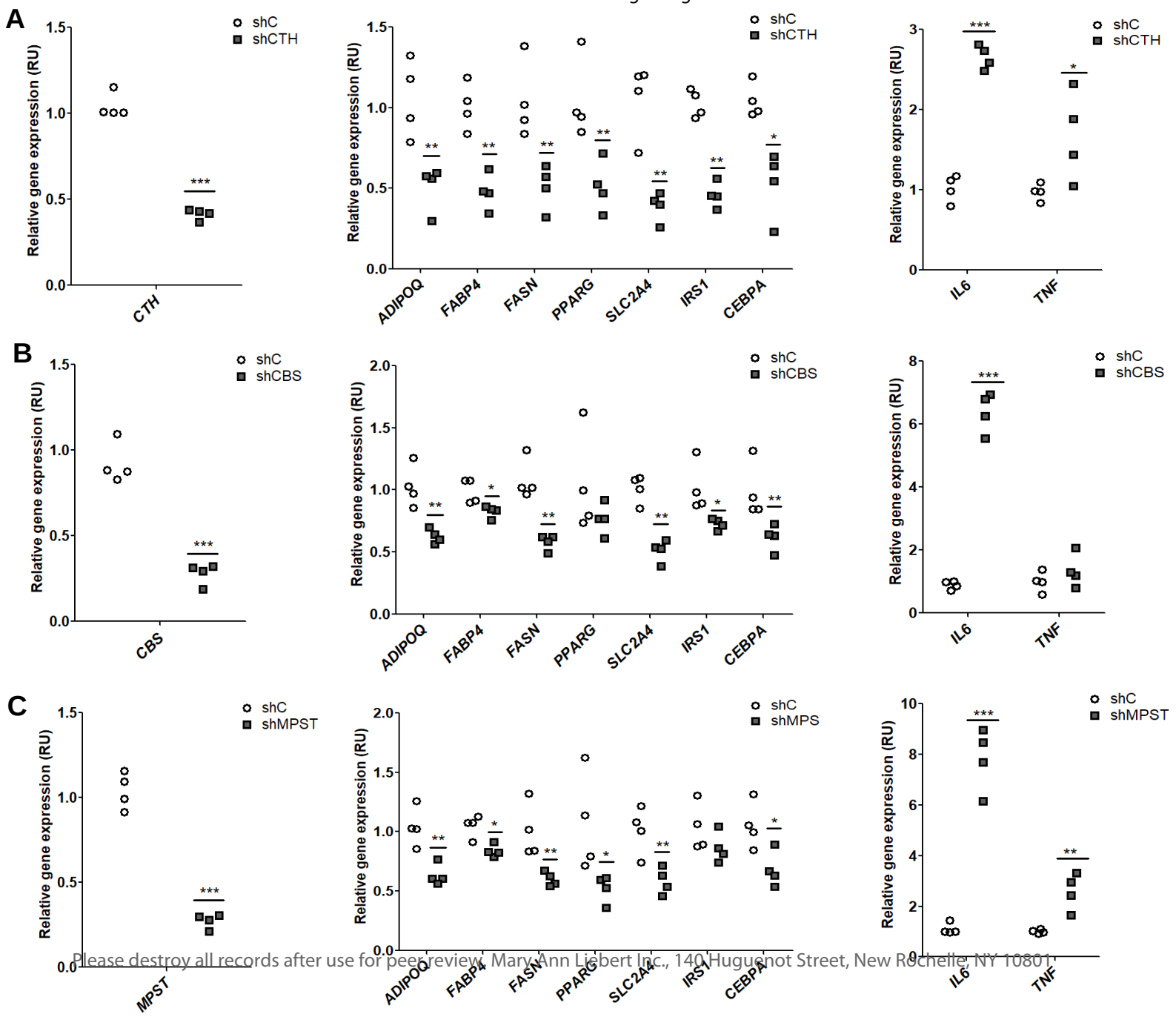

Figure 9

A

Protein persulfidation-enriched biological processes in adipocytes (%)

#Term ID	Term description	%	FDR
GO:0006085	acetyl-CoA biosynthetic process	69.23	1.9E-10
GO:0033539	fatty acid beta-oxidation using acyl-CoA dehydrogenase	60.00	4.71E-10
GO:0006084	acetyl-CoA metabolic process	51.85	5.79E-15
GO:0006099	tricarboxylic acid cycle	50.00	6.83E-17
GO:0006101	citrate metabolic process	47.22	1.32E-17
GO:0072350	tricarboxylic acid metabolic process	45.00	2.58E-18
GO:0071616	acyl-CoA biosynthetic process	43.90	3.62E-18
GO:0006635	fatty acid beta-oxidation	41.07	1.53E-22
GO:0019395	fatty acid oxidation	32.00	1.56E-21
GO:0009060	aerobic respiration	30.99	1.34E-19
GO:0009062	fatty acid catabolic process	29.76	8.78E-22
GO:0006695	cholesterol biosynthetic process	29.27	1.71E-10
GO:0006637	acyl-CoA metabolic process	28.41	2.05E-21
GO:0043648	dicarboxylic acid metabolic process	25.77	1.22E-20
GO:0046364	monosaccharide biosynthetic process	25.45	1.53E-11
GO:0072329	monocarboxylic acid catabolic process	24.53	5.72E-21
GO:0006090	pyruvate metabolic process	24.24	6.84E-13
GO:0006119	oxidative phosphorylation	23.00	4.48E-18
GO:0045333	cellular respiration	22.88	2.24E-27
GO:0033875	ribonucleoside bisphosphate metabolic process	21.95	9.86E-21
GO:0034032	purine nucleoside bisphosphate metabolic process	21.95	9.86E-21
GO:0016999	antibiotic metabolic process	21.77	1.12E-20
GO:1990542	mitochondrial transmembrane transport	21.69	8.71E-14
GO:0046496	nicotinamide nucleotide metabolic process	21.50	1.54E-17
GO:0072524	pyridine-containing compound metabolic process	21.24	3.62E-18
GO:0044242	cellular lipid catabolic process	20.96	2.71E-26
GO:0042775	mitochondrial ATP synthesis coupled electron transport	20.51	6.18E-12

B

Protein persulfidation-enriched KEGG pathways in adipocytes (%)

#Term ID	Term description	%	FDR
hsa00020	Citrate cycle (TCA cycle)	63.33	8.75E-22
hsa00620	Pyruvate metabolism	56.41	2.91E-24
hsa00280	Valine, leucine and isoleucine degradation	50.00	2.02E-25
hsa00640	Propanoate metabolism	50.00	3.12E-17
hsa00071	Fatty acid degradation	47.73	4.7E-22
hsa01210	2-Oxocarboxylic acid metabolism	47.06	7.86E-09
hsa00061	Fatty acid biosynthesis	41.67	0.0000148
hsa01212	Fatty acid metabolism	39.58	7.19E-19
hsa00630	Glyoxylate and dicarboxylate metabolism	39.29	3.09E-11
hsa00380	Tryptophan metabolism	35.00	1.43E-13
hsa01200	Carbon metabolism	33.62	2.61E-36
hsa00410	beta-Alanine metabolism	32.26	1.29E-09
hsa00100	Steroid biosynthesis	31.58	0.00000567
hsa00062	Fatty acid elongation	28.00	0.00000152
hsa03320	PPAR signaling pathway	26.39	2.74E-16
hsa01040	Biosynthesis of unsaturated fatty acids	26.09	0.000014
hsa00650	Butanoate metabolism	25.00	0.00000281
hsa00220	Arginine biosynthesis	25.00	0.000096
hsa00030	Pentose phosphate pathway	23.33	0.00000404
hsa01230	Biosynthesis of amino acids	22.22	6.89E-13
hsa00010	Glycolysis / Gluconeogenesis	22.06	4.38E-12
hsa00310	Lysine degradation	22.03	1.48E-10
hsa00330	Arginine and proline metabolism	20.83	4.45E-08
hsa00190	Oxidative phosphorylation	17.56	2.74E-16
hsa00250	Alanine, aspartate and glutamate metabolism	17.14	0.0000949
hsa04714	Thermogenesis	13.60	7.19E-19
hsa04923	Regulation of lipolysis in adipocytes	13.21	0.0000912
hsa04146	Peroxisome	11.11	0.0000233
hsa04920	Adipocytokine signaling pathway	10.14	0.00035
hsa04922	Glucagon signaling pathway	9.00	0.000096
hsa04152	AMPK signaling pathway	8.33	0.0000682
hsa04910	Insulin signaling pathway	8.21	0.0000298

C

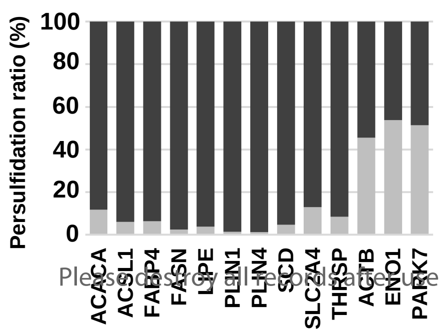

Supplementary figure legends

Suppl Figure 1. A-L) Effect of PPG (25 and 250 µM, 48h) administration on *ADIPOQ, FASN, DGAT1, PPARG, IRS1, PPARGC1A, SIRT1, BAX, TP53, IL6* and *TNF* gene expression, and on LDH activity in fully differentiated adipocytes.**p<0.01 and ***p<0.001 *vs* vehicle.

Suppl Figure 2. A-B) Protein persulfidation-enriched biological processes **(A)** and KEGG pathways **(B)** in human preadipocytes.

Suppl Figure 3. This figure includes entire blots of cropped Western blot band (in red) for CTH, MPST and CBS proteins shown in Figure 5G. Blots used to calculate mean values in densitometric analysis are shown in a green frame.

Suppl Figure 4. This figure includes entire blots of cropped Western blot band (in red) for FAS and β-actin proteins shown in Figure 5G. Blots used to calculate mean values in densitometric analysis are shown in a green frame.

Suppl Figure 5. This figure includes entire blots of cropped Western blot band (in red) for ^{pSer473}Akt and Akt proteins shown in Figure 6E. Blots used to calculate mean values in densitometric analysis are shown in a green frame.

Suppl Figure 6. This figure includes entire blots of cropped Western blot band (in red) for FAS and β-actin proteins shown in Figure 7B. Blots used to calculate mean values in densitometric analysis are shown in a green frame.

Suppl Figure 7. This figure includes entire blots of cropped Western blot band (in red) for ^{pSer536}NFκB, NFκB and β-actin proteins shown in Figure 7M. Blots used to calculate mean values in densitometric analysis are shown in a green frame.

Suppl Figure 8. This figure includes entire blots of cropped Western blot band (in red) for ^{pSer473}Akt, Akt and β-actin proteins shown in Figure 7N. Blots used to calculate mean values in densitometric analysis are shown in a green frame.

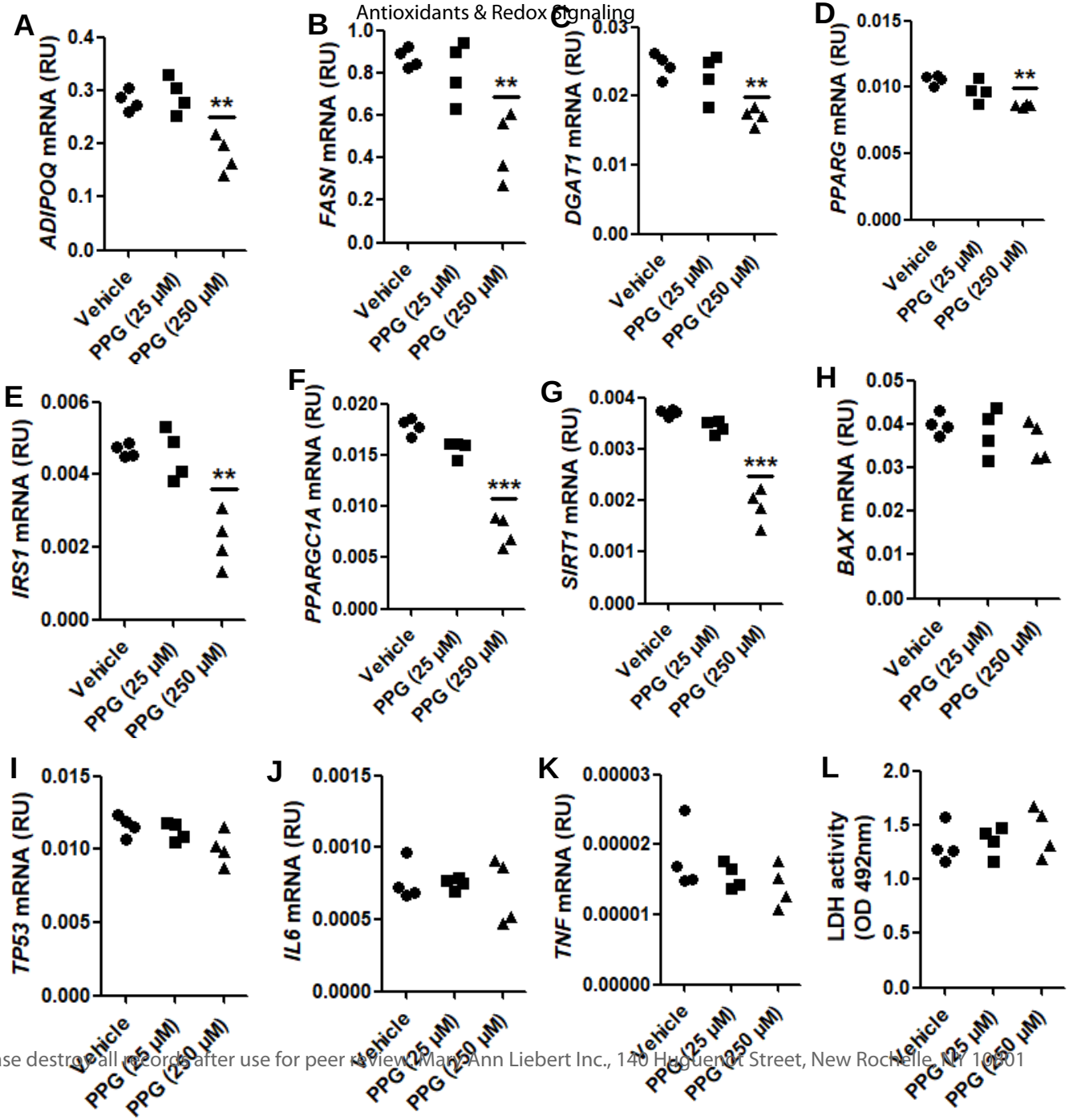

Suppl Figure 2

A

Protein persulfidation-enriched biological processes in preadipocytes (%)

#Term ID	Term description	%	FDR
GO:0002576	platelet degranulation	15.50	5.46E-11
GO:0002446	neutrophil mediated immunity	10.84	8.49E-24
GO:0043312	neutrophil degranulation	10.72	1.09E-22
GO:0002444	myeloid leukocyte mediated immunity	10.60	8.47E-24
GO:0036230	granulocyte activation	10.56	7.65E-23
GO:0043299	leukocyte degranulation	10.45	1.09E-22
GO:0045055	regulated exocytosis	10.42	5.97E-31
GO:0002275	myeloid cell activation involved in immune response	10.21	2.47E-22
GO:0002443	leukocyte mediated immunity	9.65	1.36E-24
GO:0002274	myeloid leukocyte activation	9.58	4.44E-22
GO:0006887	exocytosis	9.43	3.7E-29
GO:0002263	cell activation involved in immune response	8.87	1.16E-20
GO:0002366	leukocyte activation involved in immune response	8.77	4.82E-20
GO:0032940	secretion by cell	7.92	3.76E-26
GO:0097435	supramolecular fiber organization	7.83	8.64E-10
GO:0002252	immune effector process	7.77	3.17E-24
GO:0030036	actin cytoskeleton organization	7.66	3.59E-10
GO:0042060	wound healing	7.59	4.7E-11
GO:0006897	endocytosis	7.45	8.92E-12
GO:0046903	secretion	7.38	1.74E-25
GO:0045321	leukocyte activation	7.16	8.8E-20
GO:0009611	response to wounding	7.13	1.44E-11
GO:0030029	actin filament-based process	7.10	2.57E-10
GO:0016192	vesicle-mediated transport	7.06	3.78E-39
GO:0001775	cell activation	6.93	1.98E-21
GO:0098657	import into cell	6.90	4.81E-12
GO:0030334	regulation of cell migration	5.98	5.08E-11
GO:0051130	positive regulation of cellular component organization	5.85	3.4E-16
GO:0051270	regulation of cellular component movement	5.64	1.93E-11
GO:0022603	regulation of anatomical structure morphogenesis	5.62	2.55E-12
GO:0016477	cell migration	5.54	4.9E-10
GO:0048870	cell motility	5.25	5.29E-10
GO:0006955	immune response	5.06	2.58E-16
GO:0006928	movement of cell or subcellular component	5.02	1.35E-13

B

Protein persulfidation-enriched KEGG pathways in preadipocytes (%)

#Term ID	Term description	%	FDR
hsa00531	Glycosaminoglycan degradation	21.05	0.004
hsa00052	Galactose metabolism	16.13	0.0025
hsa04610	Complement and coagulation cascades	15.38	0.00000122
hsa05100	Bacterial invasion of epithelial cells	15.28	0.00000372
hsa04961	Endocrine and other factor-regulated calcium reabsorption	14.89	0.00052
hsa00520	Amino sugar and nucleotide sugar metabolism	14.58	0.00055
hsa05130	Pathogenic Escherichia coli infection	13.21	0.00073
hsa04142	Lysosome	13.01	6.43E-08
hsa04510	Focal adhesion	12.69	1.07E-11
hsa04721	Synaptic vesicle cycle	11.48	0.0013
hsa04520	Adherens junction	11.27	0.00069
hsa04810	Regulation of actin cytoskeleton	10.73	3.79E-09
hsa04145	Phagosome	10.34	0.0000025
hsa05205	Proteoglycans in cancer	10.26	3.18E-08
hsa04512	ECM-receptor interaction	9.88	0.0012
hsa04670	Leukocyte transendothelial migration	9.82	0.00014
hsa04210	Apoptosis	9.63	0.0000279
hsa05146	Amoebiasis	9.57	0.0007
hsa04144	Endocytosis	9.50	8.36E-09
hsa04540	Gap junction	9.20	0.0017
hsa04912	GnRH signaling pathway	9.09	0.0017
hsa04933	AGE-RAGE signaling pathway in diabetic complications	8.16	0.0031
hsa04611	Platelet activation	8.13	0.00085
hsa05206	MicroRNAs in cancer	8.05	0.0003
hsa04071	Sphingolipid signaling pathway	7.76	0.002
hsa04530	Tight junction	7.19	0.00069
hsa05203	Viral carcinogenesis	6.56	0.0011
hsa04015	Rap1 signaling pathway	5.42	0.0069

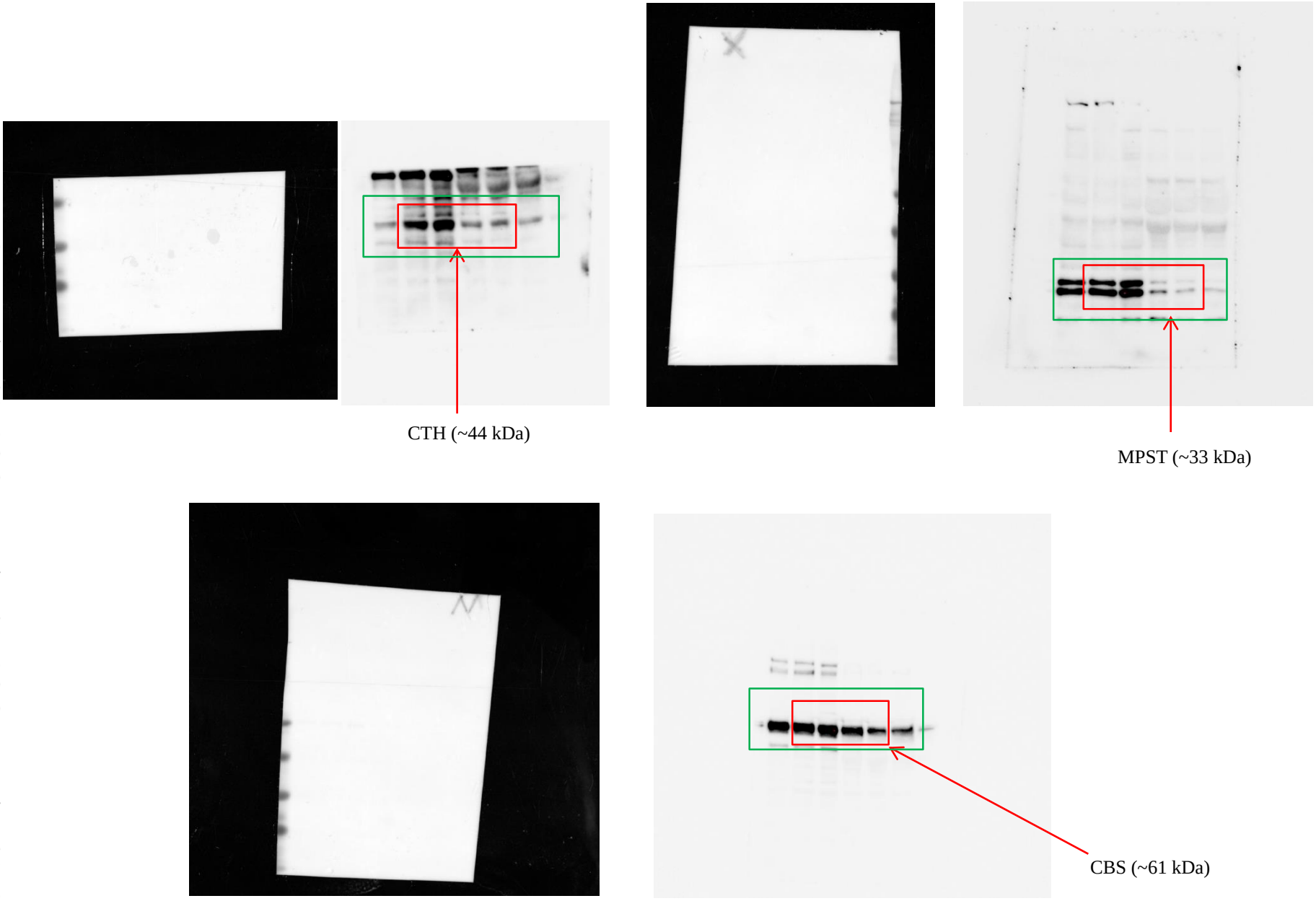

Suppl Figure 4

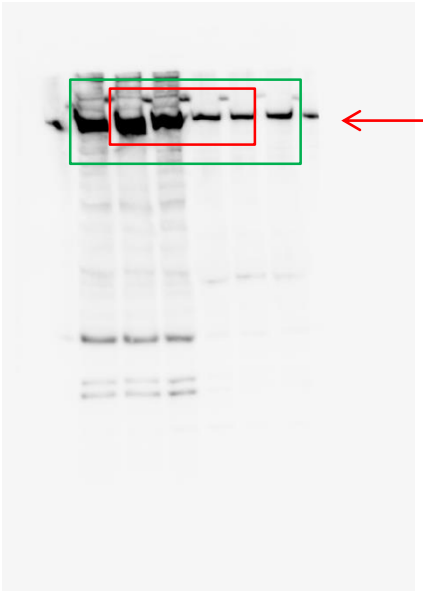

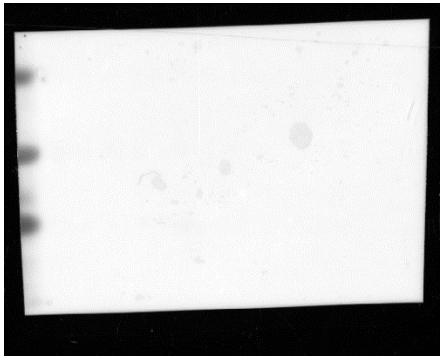

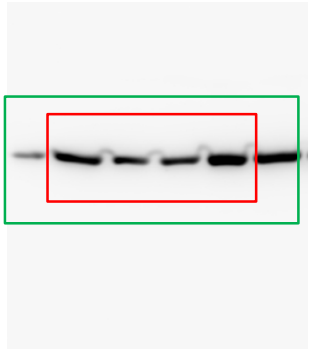

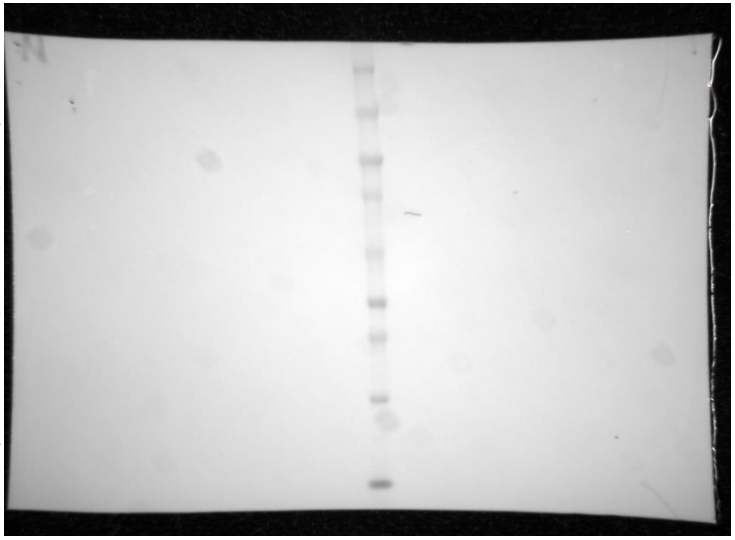

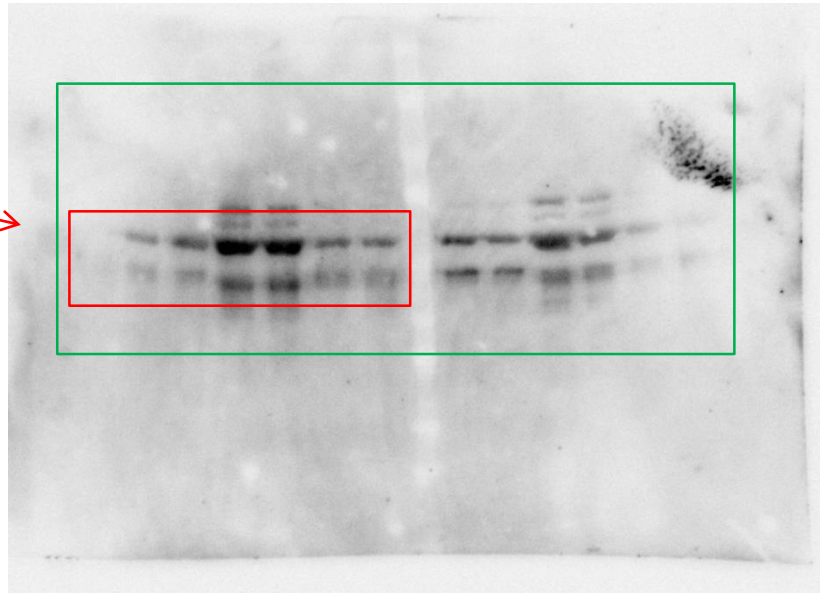

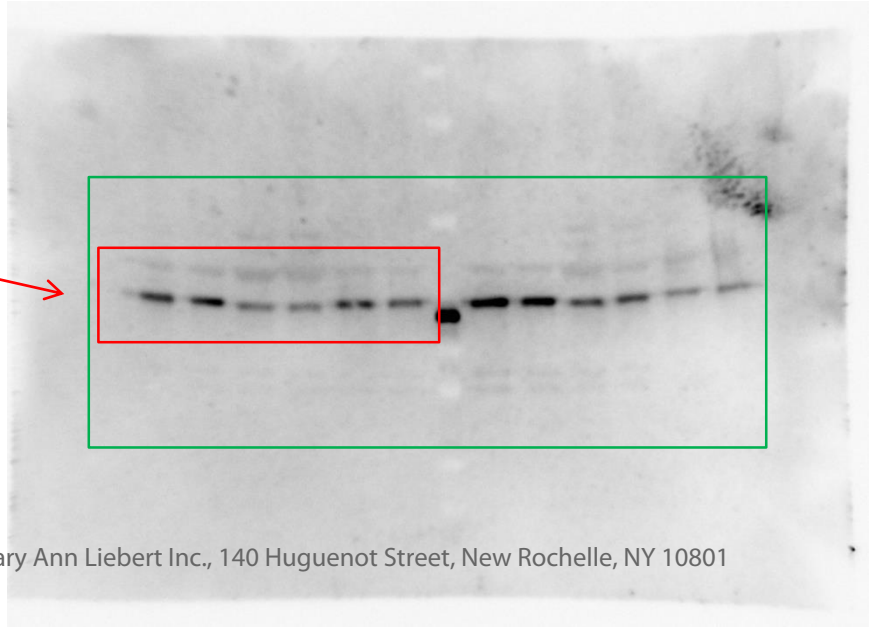

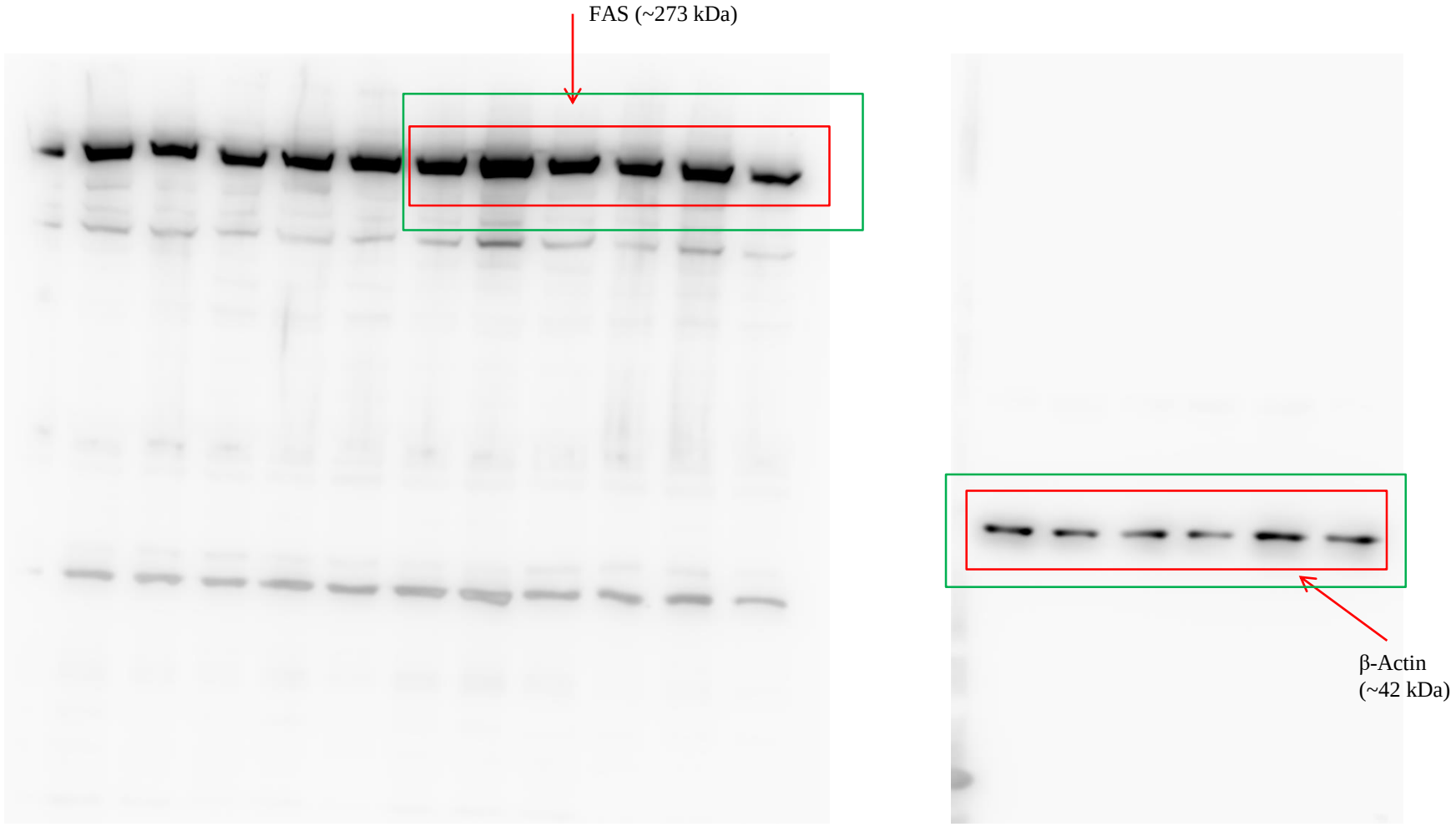

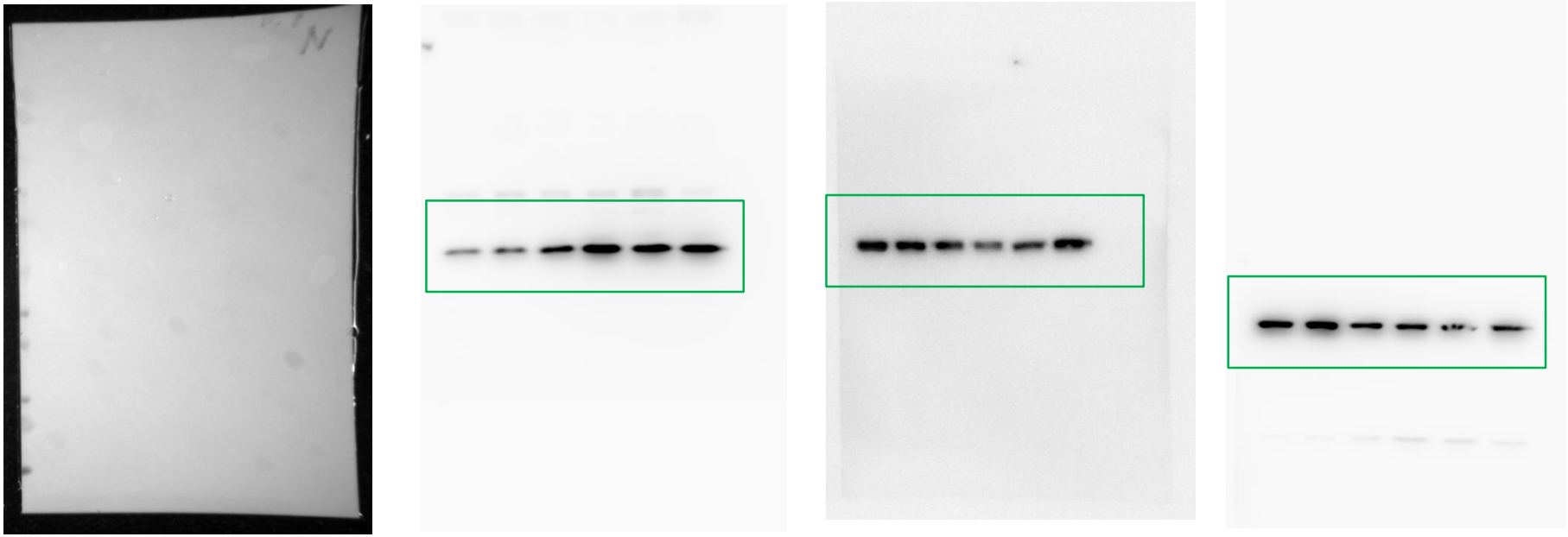

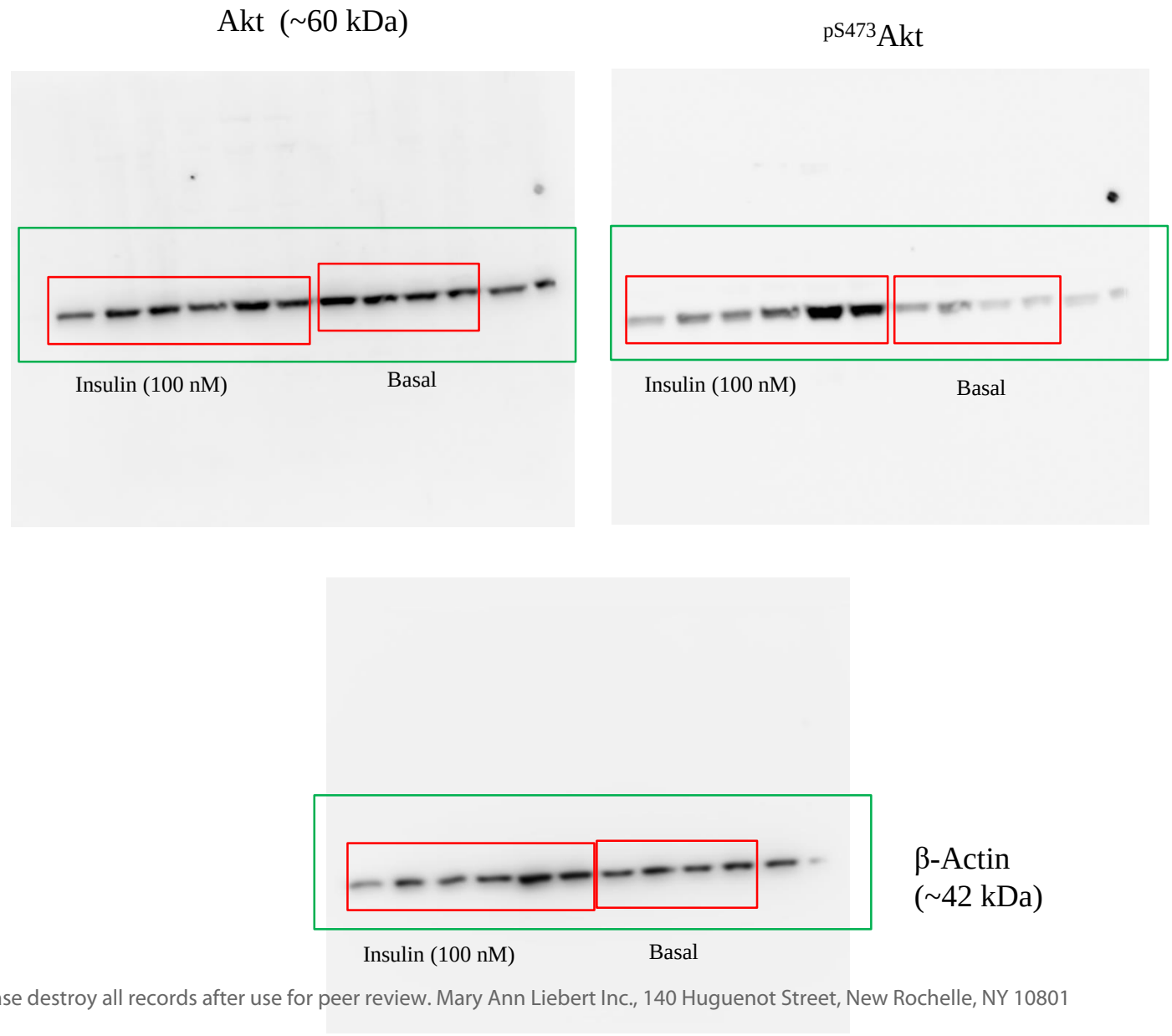

Suppl Table 1. Anthropometric and clinical characteristics of participants from *ex vivo* experiment in cohort 1.

	All participants
N	20
Age (years)	45.6 ± 9.7
BMI (kg/m^2)	44.9 ± 5.1
Waist circumference (cm)	123.9 ± 12.1
Fasting Glucose (mg/dL)	100.4 ± 13.2
HbA1c (%)	5.37 ± 0.36
M (mg/kg·min)[a]	5.73 (3.44-8.45)
Total Cholesterol (mg/dl)	181.7 ± 33.1
HDL Cholesterol (mg/dl)	50.4 ± 10.5
LDL Cholesterol (mg/dl)	111.1 ± 31.2
Fasting triglycerides (mg/dl)[a]	87 (58.2-146.2)

M, systemic insulin sensitivity measured by hyperinsulinemic-euglycemic clamp·
[a]median and interquartile range

Supp Table 2. Anthropometric and clinical characteristics in cohort 2.

	Non obese	Non obese + T2D	Obese	Obese + T2D	p-value
N	35	6	53	28	
Sex (male/female)	11/24	2/4	9/44	7/21	
Age (years)	51.1 ± 13.4	55.5 ± 13.2	45.9 ± 10.9	44.1 ± 10.4	**0.02**
BMI (kg/m^2)	25.8 ± 2.7	28.1 ± 1.3	45.1 ± 7.8$^{*\#}$	44.3 ± 5.3$^{*\#}$	**<0.0001**
Waist circumference (cm)	88.2 ± 11.1	97.6 ± 9.20	117.5 ± 20.8*	131.6 ± 14.4$^{*\#}$	**<0.0001**
Fat mass (%)	32.3 ± 5.8	36.3 ± 6.7	57.3 ± 10.1$^{*\#}$	55.2 ± 9.1$^{*\#}$	**<0.0001**
Fasting glucose (mg/dl)[a]	91 (81-98)	152.5 (99.7-210.7) *	92 (83.5-99.2) $^{\#}$	124 (92.5-167) $^{*+}$	**<0.0001**
Hb1Ac (%)	5.24 ± 0.5	8.18 ± 3.7*	4.9 ± 0.4$^{\#}$	6.1 ± 1.8$^{*\#+}$	**<0.0001**
HOMA-IR	2.3 ± 1.8	3.1 ± 0.2	2.5 ± 1.3	5.1 ± 3.1	0.1
Total Cholesterol (mg/dl)	210.7 ± 40.9	228.5 ± 47.9	189 ± 32.4	189 ± 32.4	**0.01**
HDL Cholesterol (mg/dl) [a]	57.5 (47.5-75.7)	47.5 (39-57.7)	52 (43.6-63)	51.6 (42.5-61.7)	0.5
LDL Cholesterol (mg/dl)	125.1 ± 31.4	152.5 ± 41.1	117.8 ± 29.9	106.5 ± 33.6$^{\#}$	**0.01**
Fasting triglycerides (mg/dl) [a]	98 (76.2-154.5)	160 (105-220)	98 (75.2-131.7)	125.5 (90.5-172)	0.1
VAT *CTH* (R.U.)	0.0041 ± 0.002	0.0026 ± 0.001	0.0021 ± 0.001*	0.0016 ± 0.0007*	**<0.0001**
SAT *CTH* (R.U.)	0.0040 ± 0.002	0.0026 ± 0.001	0.0016 ± 0.0008*	0.0017 ± 0.0007*	**<0.0001**
VAT *CBS* (R.U.)	0.0087 ± 0.006	0.0055 ± 0.003	0.0039 ± 0.002*	0.0046 ± 0.002*	**<0.0001**
SAT *CBS* (R.U.)	0.0045 ± 0.003	0.0021 ± 0.001*	0.0017 ± 0.0008*	0.0017 ± 0.0007*	**<0.0001**
VAT *MPST* (R.U.)	0.0315 ± 0.018	0.0222 ± 0.001	0.0265 ± 0.012	0.0252 ± 0.012	0.1
SAT *MPST* (R.U.)	0.0423 ± 0.023	0.0245 ± 0.016*	0.0301 ± 0.014*	0.0255 ± 0.009^{*+}	**<0.0001**

VAT, visceral adipose tissue; SAT, subcutaneous adipose tissue; T2D, Type 2 Diabetes; HOMA-IR, Homeostasis Model Assessment – Insulin Resistance Index; R.U., relative gene expression units.
[a]median and interquartile range
*p<0.05 compared to non obese participants after performing Bonferroni post hoc test.
# p<0.05 compared to non obese participants with type 2 diabetes after performing Bonferroni post hoc test.
+ p<0.05 compared to obese participants after performing Bonferroni post hoc test.

Suppl Table 3. Anthropometric and clinical characteristics in cohort 3.

	Obese	Obese + T2D	p-value
N	19	16	
Sex (male/female)	5/14	3/13	
Age (years)	47.2 ± 9.8	49.8 ± 8.1	0.4
BMI (kg/m^2)	42.9 ± 6.4	46.5 ± 6.5	0.1
WHR	0.89 (0.77-1.01)	0.88 (0.83-0.91)	0.3
M (mg/kg·min)	4.55 ± 2.5	3.11 ± 1.7	0.1
Fasting glucose (mg/dl)	94 (85.7 – 98.2)	113 (97.5-140)	**0.03**
Hb1Ac (%)	5.60 ± 0.4	7.02 ± 1.8	**0.01**
Total Cholesterol (mg/dl)	194.6 ± 36.8	175 ± 33.9	0.1
HDL Cholesterol (mg/dl)	46.3 ± 8.3	51.6 ± 18.3	0.2
LDL Cholesterol (mg/dl)	125.6 ± 29.3	96.6 ± 29.6	**0.008**
Fasting triglycerides (mg/dl)	113 ± 49.3	133.7 ± 66.2	0.2

Suppl Table 4. Persulfidated proteins indetified in the spectral library only pr

TBA1B_HUMAN
GANAB_HUMAN
COCA1_HUMAN
VDAC2_HUMAN
ADT3_HUMAN
J3QSU6_HUMAN
A0A0A0MT01_HUMAN
H7C3P4_HUMAN
A0A0A0MSQ0_HUMAN
ACTA_HUMAN
OPLA_HUMAN
E9PLK3_HUMAN
A0A024R571_HUMAN
PARK7_HUMAN
G5E977_HUMAN
EF1D_HUMAN
K7EK35_HUMAN
K7ELL7_HUMAN
B1AK88_HUMAN
E9PK25_HUMAN
ILK_HUMAN
M0QXF9_HUMAN
G8JLB6_HUMAN
A0A1B0GUH5_HUMAN
H7C003_HUMAN
A0A096LPI6_HUMAN
GSTK1_HUMAN
A0A1B0GW77_HUMAN
J3QTR3_HUMAN
E7EUU4_HUMAN
RAB1A_HUMAN
H0Y2Y8_HUMAN
TOM40_HUMAN
F5H5P2_HUMAN
H0YL69_HUMAN
HSDL2_HUMAN
Q5STU3_HUMAN
A0A1W2PQH3_HUMAN
TIM44_HUMAN
A0A2R8Y4T1_HUMAN
G3V1D3_HUMAN
C9JRZ6_HUMAN
ARK72_HUMAN
NDUA9_HUMAN
PDLI5_HUMAN

C9JMB8_HUMAN
HMCS1_HUMAN
H3BN98_HUMAN
E7ETB3_HUMAN
K2C79_HUMAN
GSTM1_HUMAN
A6NP24_HUMAN
SDHB_HUMAN
TECR_HUMAN
S10A9_HUMAN
A0A2R8YDQ9_HUMAN
A8K968_HUMAN
ABHEB_HUMAN
I3L2B0_HUMAN
TMED4_HUMAN
H2A1C_HUMAN
ACTBL_HUMAN
MUTA_HUMAN
H0YK42_HUMAN
NDUS7_HUMAN
CHP1_HUMAN
PMVK_HUMAN
H2B1H_HUMAN
TOM22_HUMAN
AT5F1_HUMAN
SAM50_HUMAN
AKAP2_HUMAN
A0A2R8Y891_HUMAN
CBPM_HUMAN
PPAL_HUMAN
H3BPK3_HUMAN
E9PK52_HUMAN
DEST_HUMAN
E7EPB3_HUMAN
RAB18_HUMAN
NUCL_HUMAN
H7C1D4_HUMAN
MMAB_HUMAN
MARC1_HUMAN
E9PJH7_HUMAN
DUS23_HUMAN
RL10A_HUMAN
MYG1_HUMAN
DHRS4_HUMAN
PXDN_HUMAN
COPG2_HUMAN

ARP5L_HUMAN
H0YIV4_HUMAN
H7C3M2_HUMAN
A0A2U3TZJ9_HUMAN
K2C6B_HUMAN
F5H5D3_HUMAN
NU5M_HUMAN
RM18_HUMAN
A0A2R8Y7C0_HUMAN
EIF3D_HUMAN
E9PNQ8_HUMAN
RS10_HUMAN
ACAD8_HUMAN
M0R2F8_HUMAN
F8VS07_HUMAN
PGES2_HUMAN
H0YNX5_HUMAN
F8VXI1_HUMAN
A6NKE1_HUMAN
SGMR1_HUMAN
CCD47_HUMAN
LTOR5_HUMAN
CAVN2_HUMAN
DCMC_HUMAN
C9JXA5_HUMAN
ACSL3_HUMAN
ELOV1_HUMAN
S10A7_HUMAN
FA49B_HUMAN
COASY_HUMAN
H3BS72_HUMAN
H0YD13_HUMAN
S2546_HUMAN
ADPGK_HUMAN
BCS1_HUMAN
CDN2C_HUMAN
A6NIW2_HUMAN
2A5A_HUMAN
RS2_HUMAN
F1T0B3_HUMAN
TBB2A_HUMAN
A0A0C4DFV9_HUMAN
J3KPF3_HUMAN
PA2G4_HUMAN
K7EQ77_HUMAN
UFD1_HUMAN

THEM6_HUMAN
A0A0A0MQV1_HUMAN
D2HDH_HUMAN
IF2M_HUMAN
K7ERI7_HUMAN
VAS1_HUMAN
G3XAM7_HUMAN
A0A087WZF1_HUMAN
H7C2P7_HUMAN
H0YF29_HUMAN
F8VXZ8_HUMAN
BID_HUMAN
F6XZQ7_HUMAN
ILF2_HUMAN
K4DI93_HUMAN
TGBR3_HUMAN
H3BT57_HUMAN
TMX2_HUMAN
PIGS_HUMAN
THTM_HUMAN
GLRX3_HUMAN
RD23A_HUMAN
H0Y3P2_HUMAN
RPE_HUMAN
MEP50_HUMAN
ALAT1_HUMAN
H3BRV9_HUMAN
E9PPC8_HUMAN
PTN11_HUMAN
NIT1_HUMAN
F5GYF7_HUMAN
NOP56_HUMAN
CCD51_HUMAN
RUXF_HUMAN
J9JIE6_HUMAN
F8W031_HUMAN
A6NF51_HUMAN
F5H1S8_HUMAN
PHLB1_HUMAN
B4E1G1_HUMAN
C9J0G0_HUMAN
E9PR47_HUMAN
B1AK20_HUMAN
GPC1_HUMAN
AMRP_HUMAN
A0A087WT99_HUMAN

USMG5_HUMAN
A0A0A0MRN5_HUMAN
A0A087WVC4_HUMAN
SORT_HUMAN
RM21_HUMAN
H3BPJ9_HUMAN
F5GZY1_HUMAN
IGSF8_HUMAN
EFTS_HUMAN
D6RAA6_HUMAN
RS11_HUMAN
CLPT1_HUMAN
INF2_HUMAN
NDUA2_HUMAN
M0R0X1_HUMAN
RAB4B_HUMAN
RAB4A_HUMAN
NEXN_HUMAN
K7ELX4_HUMAN
E9PRK8_HUMAN
F1T0I1_HUMAN
PPME1_HUMAN
AT131_HUMAN
SYYM_HUMAN
CLMN_HUMAN
GOGB1_HUMAN
G3V3Y1_HUMAN
PPOX_HUMAN
PUR4_HUMAN
OSB11_HUMAN
B7WPE2_HUMAN
CLYBL_HUMAN
NDK3_HUMAN
YIPF6_HUMAN
FIS1_HUMAN
SYCM_HUMAN
CAH5B_HUMAN
PAIRB_HUMAN
PRKRA_HUMAN
H0YHG0_HUMAN
Q5T985_HUMAN
CC177_HUMAN
B5MBZ0_HUMAN
HERC1_HUMAN
I3L294_HUMAN
LPIN1_HUMAN

D6RDG3_HUMAN
C9K057_HUMAN
A0A0A0MRL7_HUMAN
ABCD3_HUMAN
H0Y962_HUMAN
H0Y8C3_HUMAN
E9PPJ0_HUMAN
E9PM75_HUMAN
LANC2_HUMAN
GRB2_HUMAN
RASF9_HUMAN
RBL2_HUMAN
F8W914_HUMAN
H7C4C5_HUMAN
RAB13_HUMAN
PIPSL_HUMAN
A0A0C4DG90_HUMAN
G3V274_HUMAN
G0XQ39_HUMAN
Q5W015_HUMAN
G3V2V6_HUMAN
NU133_HUMAN
RLA1_HUMAN
E9PI90_HUMAN
J3KN16_HUMAN
G3V5T0_HUMAN
A0A087WW43_HUMAN
PSB7_HUMAN
HECD3_HUMAN
M0R2C6_HUMAN
L7N2F4_HUMAN
K7EL62_HUMAN
J3QLD9_HUMAN
H7C5Q9_HUMAN
H3BM30_HUMAN
H0YL43_HUMAN
H0YH33_HUMAN
B5MDD7_HUMAN
B1AH87_HUMAN
A0A2R8YE10_HUMAN
OVCA2_HUMAN
PYRD_HUMAN
CRKL_HUMAN
OSBP1_HUMAN
AIP_HUMAN
S35U4_HUMAN

Q5TBR1_HUMAN
Q5T196_HUMAN
M0R0I3_HUMAN
I3L4C3_HUMAN
I3L448_HUMAN
H7C5K4_HUMAN
H7C5F5_HUMAN
H3BQR2_HUMAN
H0YI20_HUMAN
G5E9F5_HUMAN
G3V158_HUMAN
F8WAS2_HUMAN
C9JN98_HUMAN
B5MD00_HUMAN
B1AJY7_HUMAN
A0A0A0MR74_HUMAN
MINP1_HUMAN
NPS3A_HUMAN
S10AE_HUMAN
NUD16_HUMAN
NANP_HUMAN
RM10_HUMAN
K1614_HUMAN
S2535_HUMAN
TBR1_HUMAN
GUAA_HUMAN
RARG_HUMAN
ATP6_HUMAN
RFPL3_HUMAN
QCR10_HUMAN
NKX26_HUMAN
F172B_HUMAN
B8ZZ31_HUMAN
V9GYL9_HUMAN
I3L4J1_HUMAN
GALT2_HUMAN
NUCG_HUMAN
E5RJD8_HUMAN
NFU1_HUMAN
NUCB1_HUMAN
DHTK1_HUMAN
RS26_HUMAN
H0Y2W2_HUMAN
WDR13_HUMAN
SC24B_HUMAN
ARI2_HUMAN

H3BN14_HUMAN
A0A0A0MQS1_HUMAN
CLIP2_HUMAN
F8WBJ7_HUMAN
C9JQ42_HUMAN
F8W7Q4_HUMAN
LEG7_HUMAN
PGP_HUMAN
L2HDH_HUMAN
G5E9Q6_HUMAN
EFGM_HUMAN
MGAT1_HUMAN
COX5B_HUMAN
NDUS6_HUMAN
PECR_HUMAN
H7C2W1_HUMAN
ANPRA_HUMAN
G3V1R5_HUMAN
H7BYH4_HUMAN
RALB_HUMAN
SRP68_HUMAN
H7BZM7_HUMAN
DNJA3_HUMAN
TCP4_HUMAN
A0A024RBT2_HUMAN
CALL3_HUMAN
F5H8H2_HUMAN
D3YTC7_HUMAN
PLAP_HUMAN
E9PR30_HUMAN
E9PRQ3_HUMAN
HPRT_HUMAN
H0Y2X5_HUMAN
H7C0X4_HUMAN
NACAM_HUMAN
A0A0A0MTN0_HUMAN
TMLH_HUMAN
A0A0G2JRQ5_HUMAN
RT36_HUMAN
RRFM_HUMAN
RT21_HUMAN
H7C5U8_HUMAN
PPCS_HUMAN
RM14_HUMAN
V9GYM8_HUMAN
FKBP2_HUMAN

VAPA_HUMAN
A6PVN9_HUMAN
Q5T948_HUMAN
F6WIT2_HUMAN
A6PVN5_HUMAN
PTPA_HUMAN
A6PVN7_HUMAN
F8WEJ5_HUMAN
PLPHP_HUMAN
C9JYY9_HUMAN
E9PNR9_HUMAN
SNX5_HUMAN
J3QLR8_HUMAN
R4GNH9_HUMAN
H3BV90_HUMAN
ERLEC_HUMAN
H0YJT9_HUMAN
H7C2N7_HUMAN
F8WCZ6_HUMAN
MLF2_HUMAN
SPR2G_HUMAN
AT5EL_HUMAN
CASC3_HUMAN
K7EKE5_HUMAN
A0A2R8Y5M6_HUMAN
Q5T7C4_HUMAN
E9PIF4_HUMAN
PTCD3_HUMAN
H3BNI9_HUMAN
M0R2A0_HUMAN
FSTL1_HUMAN
PGTA_HUMAN
H7C2L8_HUMAN
M1IP1_HUMAN
K7ES31_HUMAN
CIA2A_HUMAN
J3KRZ4_HUMAN
SAR1B_HUMAN
A0A140T8W3_HUMAN
SYTM_HUMAN
K7ESP4_HUMAN
A0A1W2PNX8_HUMAN
H0YMV8_HUMAN
E7ETN3_HUMAN
TPMT_HUMAN
J3KS46_HUMAN

KDM3B_HUMAN
D6RFF8_HUMAN
B4DSN5_HUMAN
NDUF3_HUMAN
RDH13_HUMAN
K7EPK1_HUMAN
A0A286YF41_HUMAN
J3QW43_HUMAN
A0A087WU53_HUMAN
A0A087WUH5_HUMAN
LSM3_HUMAN
PGAM5_HUMAN
PFD6_HUMAN
QCR8_HUMAN
G3V533_HUMAN
G3V4X6_HUMAN
PIR_HUMAN
UB2V1_HUMAN
J3QS96_HUMAN
S38AA_HUMAN
Q573B4_HUMAN
GARE1_HUMAN
FITM2_HUMAN
ABCD2_HUMAN
B4DIH5_HUMAN
UCRIL_HUMAN
CO5A2_HUMAN
RBM25_HUMAN
H0YGW7_HUMAN
Q5QPK2_HUMAN
F8WBH5_HUMAN
KTHY_HUMAN
H0YBU9_HUMAN
K7EQ63_HUMAN
MYH14_HUMAN
ARL2_HUMAN
M0R0N4_HUMAN
IPYR2_HUMAN
A0A087X0W9_HUMAN
E5RFF0_HUMAN
RRF2M_HUMAN
DAG1_HUMAN
A1BG_HUMAN
XPP3_HUMAN
E7EWX6_HUMAN
X6RJ73_HUMAN

RDH10_HUMAN
H3BQK9_HUMAN
F8VVX6_HUMAN
E5RIM7_HUMAN
C9JS27_HUMAN
E9PAL7_HUMAN
MCTS1_HUMAN
RFIP1_HUMAN
MFN2_HUMAN
KDM5A_HUMAN
RL35A_HUMAN
PALM3_HUMAN
ADT1_HUMAN
E9PC69_HUMAN
TI23B_HUMAN
R4GN36_HUMAN
H3BQG3_HUMAN
M0QXS5_HUMAN
PRI2_HUMAN
Q5H9B5_HUMAN
UFL1_HUMAN
TRFE_HUMAN
E7EWP0_HUMAN
C9IZG4_HUMAN
PPIL1_HUMAN
GEMI5_HUMAN
LPH_HUMAN
CK068_HUMAN
RENT1_HUMAN
H1BP3_HUMAN
PGLT1_HUMAN
M0R2L2_HUMAN
E7EX17_HUMAN
LRN4L_HUMAN
S4R313_HUMAN
TACO1_HUMAN
YLAT2_HUMAN

·esent in differentiated adipocyte samples.